J_1-J_2 frustrated two-dimensional Heisenberg model: Random phase approximation and functional renormalization group

Johannes Reuther and Peter Wölfle
Institut für Theorie der Kondensierten Materie, Karlsruhe Institute of Technology, D-76128 Karlsruhe, Germany
(Received 16 December 2009; revised manuscript received 11 February 2010; published 8 April 2010)

We study the ground-state properties of the two-dimensional spin-1/2 J_1-J_2 Heisenberg model on a square lattice, within diagrammatic approximations using an auxiliary-fermion formulation with exact projection. In a first approximation, we assume a phenomenological width of the pseudofermion spectral function to calculate the magnetization, susceptibilities, and the spin-correlation length within random-phase approximation, demonstrating the appearance of a paramagnetic phase between the Néel-ordered and Collinear-ordered phases, at sufficiently large pseudofermion damping. Second we use a functional renormalization-group formulation. We find that the conventional truncation scheme omitting three-particle and higher-order vertices is not sufficient. We therefore include self-energy renormalizations in the single-scale propagator as recently proposed by Katanin, to preserve Ward identities in a better way. We find Néel order at $g=J_2/J_1 \lesssim g_{c1} \approx 0.4 \ldots 0.45$ and Collinear order at $g \gtrsim g_{c2} \approx 0.66 \ldots 0.68$, which is in good agreement with results obtained by numerical studies. In the intervening quantum paramagnetic phase, we find enhanced columnar dimer and plaquette fluctuations of equal strength.

DOI: 10.1103/PhysRevB.81.144410 PACS number(s): 75.10.Jm, 75.30.Kz, 75.50.Ee

I. INTRODUCTION

It has been known for a long time that quantum antiferromagnets, i.e., spin-1/2 systems coupled by Heisenberg exchange interaction, are strongly affected by quantum fluctuations at low temperatures. Thermal fluctuations are important as well, especially since they suppress long-range order (LRO) in two dimensions at any finite temperature but their role is relatively well understood. By contrast, quantum fluctuations operate in a much more complex way: they may suppress LRO but may at the same time lead to novel ground states known under the labels "spin liquids, valence-bond solids." The first such state proposed in the literature is Anderson's RVB—(resonating-valence-bond)—state.[1] In the context of cuprate superconductors, viewed as hole-doped Mott insulators, RVB states have been proposed by Anderson[2] to form the fundamental basis on which the theory of high-T_c superconductivity should be built. Although the idea has been considered by many authors since then, there is no conclusive answer to the question of the role of a spin-liquid state for high-temperature superconductivity. These studies have raised the question, however, under which conditions quantum fluctuations are strong enough to destroy long-range order. In general, spin-liquid-type states may be expected to be stabilized by any type of quantum fluctuations. For spin systems, it has been proposed that frustration either by competing spin interactions or due to special geometric arrangements may lead to a spin-liquid state. In particular, by tuning the interactions or the lattice anisotropy a quantum phase transition from a state with long-range order into a spin-liquid state may take place. Generally speaking it has proven to be, may be unexpectedly, hard to destroy long-range order by quantum fluctuations.

The simplest theoretical model of such a system is the quantum Heisenberg antiferromagnet with nearest-neighbor interaction for spins 1/2 on a two-dimensional square lattice. Its ground state is known to be the Néel state with staggered magnetization reduced by quantum fluctuations.[3] At any finite temperature, the magnetic order is destroyed by thermal fluctuations but the correlation length is found to increase exponentially with decreasing temperature.[4,5] This physics has also been obtained from the quantum nonlinear sigma model in the renormalized classical regime.[6]

A simple model with competing interactions is the J_1-J_2 model,[7] featuring an additional antiferromagnetic next-nearest-neighbor interaction J_2 in addition to the nearest-neighbor coupling J_1. This model has attracted attention as a simplified model[8] for the effect of doping in the cuprate superconductors when a small concentration of holes is doped into the CuO planes, the long-range AF order of the undoped system is rapidly destroyed,[9,10] giving way to a nonmagnetic "pseudogap" state and to superconductivity.

Recently, this model has also found use for certain vanadate compounds,[11,12] for which the magnetic interactions can be modeled by the J_1-J_2 Hamiltonian of weakly coupled planes.

Even more recently, the J_1-J_2 model has been invoked to account for the weakened AF long-range order in the iron pnictides.[13–15] The universally observed linear temperature dependence of the magnetic susceptibility of these compounds has also been addressed in the framework of the J_1-J_2 model.[16]

If the spins of the model are considered as classical ($S \to \infty$), there is an abrupt transition from Néel order to the Collinear configuration for sufficiently strong frustration, $J_2/J_1=1/2$. In mean-field approximation, a first-order transition from the Néel to the Collinear state is found. However, this is changed by quantum fluctuations. Early on it has been found[7,17,18] that a nonmagnetic phase exists in the region $0.4 \lesssim J_1/J_2 \lesssim 0.65$, between the two ordered states. The nature of this intermediate state is what we would like to unravel. Most recent mainly numerical work (see Refs. 19–21, and references therein) on the J_1-J_2 model indicates that it may be a valence-bond solid[22] (VBS), rather than a homoge-

neous spin liquid.[23] In the VBS, the spins in the plane form pairwise singlets, which are spontaneously dimerized in a, e.g., columnar pattern and therefore break the lattice translational symmetry. It has also been proposed that the dimerization takes place on units of 2×2 plaquettes.[24] Evidence for a VBS has also been found in studies[25,26] of a model of coupled spin chains,[27] when the results are extrapolated to the isotropic J_1-J_2 model in the plane. Concerning the nature of the quantum phase transitions recent studies indicate that the transition from the paramagnetic phase to the Collinear configuration is of first order.[19–21,28] On the other hand, the properties of the transition from the Néel phase to the paramagnetic phase are still highly controversial. Recent studies point to either a first-order[19,25] or a second-order transition.[28,29] The latter scenario gives rise to the question of how two differently ordered phases may be connected by a continuous phase transition.[30]

In this paper, we develop several analytical methods for calculating the ground states and the excitation spectra of spin models with competing interactions, such as the model discussed above, on the basis of infinite resummations of perturbation theory in the couplings J_1 and J_2. To this end, we use a representation of the spin operators in terms of pseudofermions.[31] One motivation for using a fermionic representation rather than a bosonic representation is the available experience in describing spin liquids or dimerized spin-singlet states with fermions, mainly within large-N and mean-field approaches (see, e.g., Refs. 32–35). On the other hand, pseudofermion representations have hardly been used to study magnetic ordering phenomena.[36] Although a large body of results of numerical studies of these models is available, analytical approaches starting from a microscopic Hamiltonian are rare. We use a newly developed implementation of the functional renormalization-group (FRG) method[37,38] applied to interacting quantum spin models. In this we are aided by the experience, we have previously gained with the nearest-neighbor Heisenberg model.[39,40] Auxiliary particle representations of spin operators are sometimes viewed with suspicion, as they are conceived to be fraught with uncontrolled approximations regarding the projection unto the physical sector of the Hilbert space necessary in those spin representations. Here we are using an exact method of projection onto the physical part of Hilbert space that works even on the lattice (see below).

The paper is organized as follows. Section II introduces the model, the auxiliary-fermion representation and the projection schemes in detail. Simple mean-field approximations are discussed in Sec. III where we demonstrate that these approaches are not able to capture frustration effects but rather reproduce classical results. To this end in Sec. IV, we introduce a phenomenological pseudoparticle lifetime that mimics quantum fluctuations. The results on the magnetization, susceptibilities, and spatial spin correlations show that in a certain parameter range for this lifetime, the correct phase diagram is obtained. The main part of the paper, given by Sec. V is devoted to FRG. This method enables us to calculate the auxiliary-particle damping rather than treating it as an input of the approximation. In Sec. V A, we first point out that the often applied static FRG scheme does not lead to a finite flow of the damping. Therefore in Sec. V B, in the framework of the standard truncation of the FRG equations we include the full dynamics. It turns out that within the latter (one-loop) approximation the strength of quantum fluctuations in the highly frustrated region is still underestimated, and a regime without Néel order or Collinear order is not found. We trace this deficiency of the one-loop approximation to the neglect of higher-order contributions. Another way of saying this is that the Ward identities resulting from spin conservation are badly violated in the one-loop scheme, such that not even the random-phase approximation (RPA) is reproduced in that approximation. As shown by Katanin[37] the latter problem may be remedied by using a dressed single-scale propagator, thus including three-particle correlations with nonoverlapping loops. As shown in Sec. V C, using the Katanin truncation scheme we find a phase diagram in excellent agreement with results from numerical methods. In order to investigate the properties of the nonmagnetic phase, correlation functions for columnar dimer and plaquette order are calculated in Sec. V D. We find that correlations for both kinds of dimerizations are clearly enhanced. Finally, the paper closes with a summary in Sec. VI.

It is worth mentioning that although in this first presentation of our work using the newly developed FRG method, we concentrated on demonstrating that the method is capable of giving results in agreement with results obtained mainly by purely numerical means, it should be clear that the method holds in fact considerable promise for future applications. First of all, it allows to treat thermodynamic, in contrast to finite-size systems. Second, it is ready to calculate dynamical properties (at least on the imaginary frequency axis). Third, it is easily generalized to finite temperature (work in progress). Further, it allows, in principle, to address questions of critical behavior near a quantum critical point.

II. MODEL

The effects of frustration in quantum spin models have been intensely studied in recent years. These models offer the possibility to investigate quantum phase transitions[41] between magnetically ordered and disordered phases. Especially in the context of deconfined criticality in two-dimensional spin systems,[30,42] quantum phase transitions are the object of renewed interest. A standard model capturing these phenomena is the spin-1/2 Heisenberg model on a square lattice with an antiferromagnetic nearest-neighbor coupling $J_1>0$ and a frustrating next-nearest-neighbor coupling $J_2\geq 0$, see Refs. 7, 17–24, 28, 29, and 43–51,

$$H = J_1 \sum_{nn} \mathbf{S}_i \cdot \mathbf{S}_j + J_2 \sum_{nnn} \mathbf{S}_i \cdot \mathbf{S}_j. \tag{1}$$

As far as the ground state of the model is concerned, two limiting cases are well understood. For $J_2=0$, the system is in a Néel-ordered phase with a magnetization of $\sim 60\%$ of the saturation magnetization. In the limit $g=\frac{J_2}{J_1}\to\infty$, the model reduces to two decoupled square lattices. Néel order on each of these lattices gives rise to the so-called Collinear long-range order with magnetic wave vectors $Q=(\pi,0)$ or $Q=(0,\pi)$. These two degenerate ground states correspond to

a parallel alignment of the spins along the y axis and an antiparallel alignment of neighboring spins along the x axis in the first case and vice versa in the second case. Increasing J_2 in the first limit or J_1 in the second limit leads in both cases to frustration and to a decrease in the respective order parameter, possibly all the way to zero. Indeed, the existence of a nonmagnetic phase, indicated by numerical studies, approximately in the parameter region $g \approx 0.4 \ldots 0.65$ is widely accepted.[18,20,21,28,44,46] However, the nature of the magnetically disordered phase as well as the order of the quantum phase transitions is not known with certainty so far. Candidates for this phase are a spin liquid[7,48,49] and a VBS state. For the latter, different types of order have been proposed, e.g., columnar dimer[19,28,46,51] and plaquette[21,24,28,47] order. Several studies give evidence that the transition from the nonmagnetic phase to the Collinear phase is of first order.[19–21,28,46] We also mention that in the classical large spin limit, no magnetically disordered phase exists. Instead there is a direct first-order transition between the Néel phase and the Collinear phase at $g=1/2$. In this limit, the respective magnetizations reach the saturation value.

In the past, the model has been studied with a variety of methods. Examples are: analytical approaches based on field-theory methods[22,29] or spin-wave theory;[7,17] numerical approaches such as exact diagonalization,[18,23,44,47,50] coupled cluster method,[20,45] series-expansion methods,[19,28,29,46,51] and quantum Monte Carlo method.[47,49]

In this paper, we address the ground-state properties in a rather different way. In order to allow for application of Feynman-diagram techniques,[52,53] we reformulate the problem in a fermionic language by introducing auxiliary fermions.[31,39,40] We represent the spin operators in terms of auxiliary fermions $f_{i\alpha}$,

$$S_i^\mu = \frac{1}{2}\sum_{\alpha\beta} f_{i\alpha}^\dagger \sigma_{\alpha\beta}^\mu f_{i\beta}. \tag{2}$$

Here $\sigma^\mu (\mu = x,y,z)$ are Pauli matrices, $\alpha,\beta = \uparrow,\downarrow$ are spin indices, and i is the site index. We use units with $\hbar = k_B \equiv 1$. By construction, the representation (2) satisfies the correct commutation relations. However, the Hilbert space for a single site i is now spanned by four states, of which two, representing an empty and a doubly occupied site are unphysical. The projection to the physical sector of Hilbert space is given by the auxiliary-particle constraint,

$$Q_i = \sum_\alpha f_{i\alpha}^\dagger f_{i\alpha} = 1. \tag{3}$$

We present two different projection schemes to account for this constraint.

A convenient approximate approach is to replace the constraint $Q_i=1$ by its thermodynamic average, $\langle Q_i \rangle = 1$. For a translation invariant state, the latter conditions are identical at each site, such that only a single condition remains. Since the constraint amounts to removing two of the four states per site, it is on average equivalent to half filling of the system, which in case of particle-hole symmetry is effected by applying a chemical potential $\mu=0$ to the pseudofermion system.

A different approach allowing for an exact treatment of the constraint even for lattice systems has been proposed by Popov and Fedotov.[54] It amounts to applying a homogeneous, *imaginary-valued* chemical potential $\mu^{\mathrm{PPV}} = -\frac{i\pi T}{2}$, where T is the temperature. Thus, within this scheme, the Hamiltonian H is replaced by

$$H \to H^{\mathrm{PPV}} = H - \mu^{\mathrm{PPV}} \sum_i Q_i. \tag{4}$$

Note that H denotes the Hamiltonian (1) using the representation of spin operators in Eq. (2). Given a physical operator $\mathcal{O}$ (i.e., an arbitrary sum or product of spin operators) it can be shown[40] that the expectation value $\langle \mathcal{O} \rangle^{\mathrm{PPV}}$, calculated with H^{PPV} and the *entire* Hilbert space, is identical to the physical expectation value $\langle \mathcal{O} \rangle$, where the average is performed with the original Hamiltonian H. The projection works by virtue of a mutual cancellation of the unphysical contributions of the sectors $Q_i=0$ and $Q_i=2$, at each site. It should be emphasized that although the Hamiltonian H^{PPV} is no longer Hermitian, the quantity $\langle \mathcal{O} \rangle^{\mathrm{PPV}}$ comes out real valued. If on the other hand, $\mathcal{O}$ is unphysical in the sense that it is nonzero in the unphysical sector, e.g., the operator $\mathcal{O}=Q_i$, the expectation value $\langle Q_i \rangle^{\mathrm{PPV}}$ is meaningless and one has $\langle Q_i \rangle \neq \langle Q_i \rangle^{\mathrm{PPV}}$.

This approach is applicable to spin models[40,55,56] but unfortunately it cannot be extended to cases away from half filling. Although μ^{PPV} vanishes in the limit $T \to 0$, in principle, the exact projection with $\mu = \mu^{\mathrm{PPV}}$ and the average projection with $\mu=0$ are not equivalent at $T=0$. This is due to the fact that the computation of an average $\langle \cdots \rangle^{\mathrm{PPV}}$ does not necessarily commute with the limit $T \to 0$. Nevertheless it can be expected that in the model considered here both projection schemes are identical at $T=0$. This can be understood with the following argument: starting from the physical (true) ground state, a fluctuation of the pseudofermion number results in two sites with unphysical occupation numbers, one with no and one with two fermions. Since these sites carry spin zero the sector of the Hamiltonian with that occupation is identical to the physical Hamiltonian where the two sites are effectively *missing*. Thus, a fluctuation from the ground state into this sector costs the binding energy of the two sites which is of the order of the exchange coupling, even in the case of strong frustration.[19–21,24,46] Consequently, at $T=0$ pseudofermion-number fluctuations are not allowed and it is sufficient to use the simpler average projection with $\mu=0$. In most calculations, we restrict ourself to this method. However, we again emphasize that at $T>0$ both schemes differ.

In the following, we will formulate approximations in terms of resummed perturbation theory in the exchange couplings J_1 and J_2. The basic building blocks are the four-fermion interactions and the bare-fermion Green's function in real space,

$$G^0_{ij,\alpha\beta}(i\omega) = \frac{1}{i\omega + \mu}\delta_{ij}\delta_{\alpha\beta}, \quad \mu = -\frac{i\pi T}{2} \quad \text{or} \quad \mu = 0. \tag{5}$$

$\omega = (2n+1)\pi T$ are the fermionic Matsubara frequencies. Note that in diagrammatic expansions, Green's functions remain

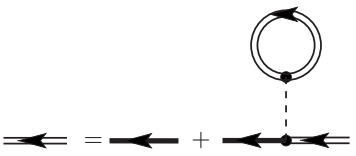

FIG. 1. Diagrammatic representation of the Hartree approximation. The full line is the bare Green's function G^0, Eq. (5) and the double-stroke line the self-consistent one. The dashed line represents the interaction J_1 or J_2 and the dots are Pauli matrices $\times 1/2$.

strictly local, i.e., $G_{ij,\alpha\beta}=\delta_{ij}G_{i,\alpha\beta}$. The momentum dependence in correlators such as the susceptibility is generated by the nonlocal exchange couplings.

We begin the calculations with a simple mean-field approach. It should be stressed that in our model, a small parameter is absent. Accordingly, a controlled summation of diagrams is a difficult task. For this reason, we extend the mean-field approach and set up a phenomenological theory which explores the consequences of certain assumptions on the width of the auxiliary-fermion spectral function and which gives qualitatively correct results.

Furthermore, the feasibility of diagrammatic approximations allows the application of the FRG method.[57–60] This scheme generates an exact, infinite hierarchy of coupled differential equations for the one-particle irreducible m-particle vertex functions by introducing an infrared cutoff. In order to be able to solve these equations numerically, one truncates the hierarchy of equations. The truncation is expected to give good results for not too strong interaction. It will turn out that the truncation procedure is a nontrivial problem for the model considered here. Effectively FRG sums up infinite classes of diagrams. This is a crucial property in the present problem for which a small parameter does not exist.

So far, FRG has been applied to low-dimensional, interacting fermion systems, e.g., the two-dimensional Hubbard model,[58,61] the single-impurity Anderson model,[62] and the Luttinger liquid with impurities[63] but a pure spin model has not been tackled with FRG.

III. MEAN-FIELD THEORY

The most elementary approximation for a spin model is the mean-field theory. In our fermionic description, it corresponds to the Hartree approximation shown in Fig. 1. The closed loop of the renormalized propagator acts as the self-consistent mean field.

Note that the Fock term is exactly zero since the nonlocal exchange coupling connects two points of the same fermion line. Dropping the requirement of exact projection, one may allow for fermion hopping and make a mean-field ansatz with nonlocal propagators. The corresponding symmetry-broken phase is the so-called RVB (Ref. 2) or the flux phase.[32,64] We will not consider mean-field amplitudes violating the auxiliary-particle constraint in this paper.

By contrast, the magnetic order parameter $\langle \mathbf{S}_i \rangle = \frac{1}{2}\Sigma_{\alpha\beta}\langle f^{\dagger}_{i\alpha}\boldsymbol{\sigma}_{\alpha\beta}f_{i\beta}\rangle$ that appears in the Hartree approximation is a physical quantity. In the following calculation, we also consider finite temperatures. Dyson's equation in Fig. 1 reads

$$\bar{G}_i(i\omega) = [(i\omega+\mu)\mathbb{1} - \bar{\Sigma}_i(i\omega)]^{-1}, \tag{6}$$

where $\bar{G}$, $\bar{\Sigma}$, and $\mathbb{1}$ are matrices in spin space. The self-energy is coupled back to the renormalized Green's function by

$$\bar{\Sigma}_i(i\omega) = \frac{1}{4}\sum_j J_{ij}\sum_{\mu=1}^{3}\sigma^{\mu}\frac{1}{\beta}\sum_{i\omega'}\mathrm{Tr}[\sigma^{\mu}\bar{G}_j(i\omega')]e^{i\omega'\delta}. \tag{7}$$

The couplings are written in the form J_{ij}, which is J_1 if i,j are nearest neighbors, and J_2 if i,j are next-nearest neighbors. The factor $e^{i\omega\delta}$, with an infinitesimal $\delta>0$, is needed for the convergence of the Matsubara sum. If we assume magnetism along the z direction, the self-energy has the form

$$\bar{\Sigma}_i(i\omega) = \sigma^z m_i. \tag{8}$$

To describe Néel and Collinear order, we split the lattice up into two sublattices A and B. In case of Néel order, A and B form a staggered pattern while for Collinear order, they form rows (or equivalently columns). Furthermore, we require

$$m \equiv m_{i\in A} = -m_{i\in B}. \tag{9}$$

Inserting Eq. (6) into Eq. (7) and using Eq. (8) one obtains

$$m_i = \frac{1}{4}\sum_j J_{ij}\frac{1}{\beta}\sum_{i\omega}\sum_{\zeta=\pm 1}\frac{\zeta}{i\omega+\mu-\zeta m_j}e^{i\omega\delta}. \tag{10}$$

Using $\frac{1}{\beta}\Sigma_{i\omega}\frac{e^{i\omega\delta}}{i\omega-z}=f(z)$ and $f(z-\mu^{\mathrm{ppv}})=\frac{1}{ie^{\beta z}+1}$ (f is the Fermi function), one finds the following self-consistent equations for m for both types of order and both projection schemes,

$$\text{Néel order: } m = \begin{cases} (J_1-J_2)\tanh\left(\frac{m\beta}{2}\right) & \text{for } \mu=0 \\ (J_1-J_2)\tanh(m\beta) & \text{for } \mu=\mu^{\mathrm{ppv}} \end{cases}, \tag{11a}$$

$$\text{Collinear order: } m = \begin{cases} J_2\tanh\left(\frac{m\beta}{2}\right) & \text{for } \mu=0 \\ J_2\tanh(m\beta) & \text{for } \mu=\mu^{\mathrm{ppv}} \end{cases}. \tag{11b}$$

The spin polarization or, in short, magnetization M_i is given by

$$M_i = \langle S^z_i\rangle = \frac{1}{2}\frac{1}{\beta}\sum_{i\omega}\mathrm{Tr}[\sigma^z\bar{G}_i(i\omega)]e^{i\omega\delta}. \tag{12}$$

From the comparison of Eqs. (7) and (12) and using $M_{i\in A}=-M_{i\in B}$, one finds a relation between m_i and M_i,

$$m_i = \frac{1}{2}\sum_j J_{ij}M_j = \begin{cases} 2M_i(J_2-J_1) & \text{for Néel order} \\ -2M_iJ_2 & \text{for Collinear order} \end{cases}. \tag{13}$$

From Eqs. (11a) and (11b), the critical temperatures $T_c^{\text{Néel}}$ and T_c^{Col} can be determined. The instability with the larger transition temperature controls the type of order at a given $g=\frac{J_2}{J_1}$. This leads to

$$0 \le g \le \frac{1}{2}: T_c = T_c^{\text{Néel}} = \begin{cases} \frac{J_1}{2}(1-g) & \text{for} \quad \mu = 0 \\ J_1(1-g) & \text{for} \quad \mu = \mu^{\text{ppv}} \end{cases}, \tag{14a}$$

$$g \ge \frac{1}{2}: T_c = T_c^{\text{Col}} = \begin{cases} \frac{J_1}{2} g & \text{for} \quad \mu = 0 \\ J_1 g & \text{for} \quad \mu = \mu^{\text{ppv}} \end{cases}. \tag{14b}$$

Apparently, within this approximation, no nonmagnetic phase is found at $T=0$. Instead there is a first-order transition from Néel to Collinear order at $g=\frac{1}{2}$. The magnetization $M=|M_i|$, which can be obtained from Eqs. (11a), (11b), and (13), reaches the saturation value $M=\frac{1}{2}$ at $T=0$, and the classical large spin behavior is reproduced. These properties hold for both projection schemes. However, this is no longer the case for $T>0$. The contribution of unphysical states with $S=0$ leads to a reduction in the magnetization in the average projection scheme. Also the critical temperatures come out a factor of two smaller in the average projection scheme. The self-consistent equations for $\mu=\mu^{\text{ppv}}$ are identical to those obtained within the conventional mean-field theory in terms of spin operators, confirming that the cancellation of the unphysical states works correctly in this approximation.

In summary, the simple mean-field theory leads to a Néel phase at $g<\frac{1}{2}$ and a Collinear-ordered phase $g>\frac{1}{2}$ but is not sufficient to describe the effect of frustration in destroying magnetic order in the regime $g \approx \frac{1}{2}$.

IV. FINITE PSEUDOFERMION LIFETIME

In the mean-field approximation, the effect of fermion scattering in generating a finite lifetime is not taken into account. We now briefly discuss a phenomenological framework for the ground state, which introduces the lifetime τ as a phenomenological parameter. To this end, we model the retarded Green's function by

$$G^{\text{R}}(\omega) = \frac{1}{\omega + i\gamma}, \quad \Sigma = -i\gamma \quad \text{with} \quad \gamma = \frac{1}{\tau}. \tag{15}$$

The spectral function $\rho(\omega)$ acquires a finite width γ,

$$\rho(\omega) = -\frac{1}{\pi} \text{Im}\, G^{\text{R}}(\omega) = \frac{\gamma}{\pi} \frac{1}{\omega^2 + \gamma^2}. \tag{16}$$

An analytic continuation of the self-energy Σ to the upper complex half plane provides

$$\Sigma(z) = -i\gamma \quad \text{for} \quad \text{Im}\, z > 0. \tag{17}$$

Since $\rho(\omega)$ is an even function, it follows immediately from the spectral representation $G(i\omega)=\int_{-\infty}^{\infty} \frac{\rho(\epsilon)}{i\omega-\epsilon} d\epsilon$ that $G(z)$ and $\Sigma(z)$ are odd functions with vanishing real parts along the complex Matsubara axes. Thus, we obtain

$$G(i\omega) = \frac{1}{i\omega + i\gamma\, \text{sgn}(\omega)}. \tag{18}$$

To proceed, we need to specify the g dependence of the damping parameter γ. For $J_2=0$, we put γ in the form $\gamma=\tilde{\gamma} J_1$, where $\tilde{\gamma}$ is a dimensionless parameter. A similar situation is encountered for $J_1 \to 0$ and $J_2>0$, where the system is split up into two square lattices, each only with nearest-neighbor couplings J_2. Therefore, in this limit, the relation $\gamma=\tilde{\gamma} J_2$ holds. To interpolate between both limiting cases, we assume

$$\gamma(J_1, J_2) = \tilde{\gamma} J_1 \sqrt{1+g^2}. \tag{19}$$

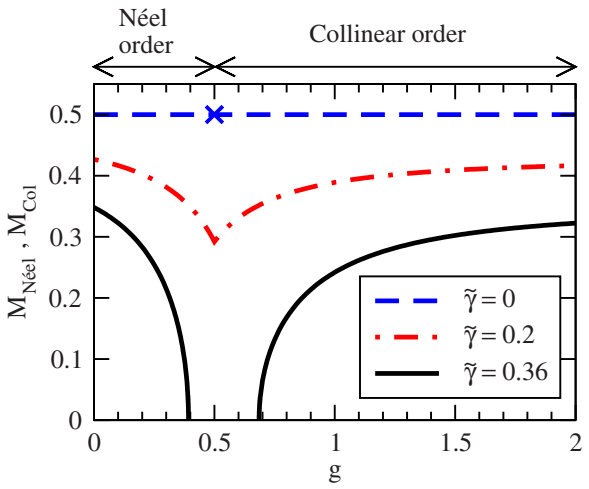

FIG. 2. (Color online) Magnetizations $M_{\text{Néel}}$ and M_{Col} versus g within the phenomenological theory for different damping parameters $\tilde{\gamma}$.

A. Hartree approximation

Replacing the bare Green's function by Eq. (18), we now calculate the ground-state magnetization within the Hartree approximation of Sec. III. In the limit $T \to 0$, using $\frac{1}{\beta}\Sigma_{i\omega} \to \frac{1}{2\pi}\int d\omega$, the new mean-field equation is given by

$$m_i = \frac{1}{4}\sum_j J_{ij} \frac{1}{2\pi} \int_{-\infty}^{\infty} d\omega \sum_{\zeta=\pm 1} \frac{\zeta}{i\omega + i\gamma\, \text{sgn}(\omega) - \zeta m_j}. \tag{20}$$

Here it is obvious that the two projection schemes are identical because a shift of the Matsubara frequencies by $\mu^{\text{ppv}}=-\frac{i\pi}{2\beta}$ becomes irrelevant in the limit $T \to 0$, provided that the Green's function, or equivalently the fermion spectral function, is regular at $\omega=0$. Equation (20) leads to the following self-consistent equations for the Néel and Collinear magnetizations,

$$M_{\text{Néel}} = \frac{1}{\pi} \arctan\left[\frac{2M_{\text{Néel}}(J_1 - J_2)}{\gamma}\right], \tag{21a}$$

$$M_{\text{Col}} = \frac{1}{\pi} \arctan\left(\frac{2M_{\text{Col}} J_2}{\gamma}\right). \tag{21b}$$

The solutions of these equations are shown in Fig. 2 for different parameters $\tilde{\gamma}$. The case $\tilde{\gamma}=0$ represents the Hartree approximation from Sec. III. An increase in $\tilde{\gamma}$ reduces the magnetizations, especially in the region of high frustration. In particular, for small $\tilde{\gamma}$, there is still a direct transition between the two types of order at $g=\frac{1}{2}$ while for sufficiently

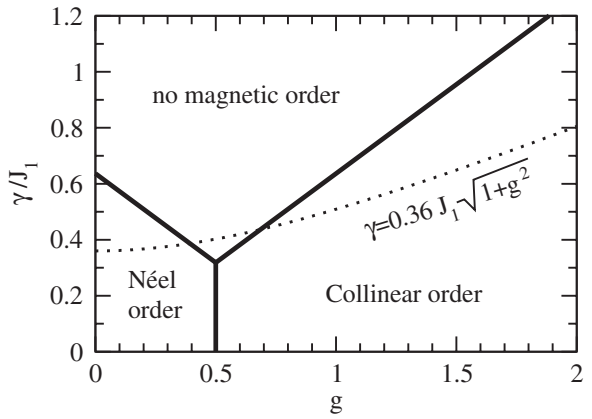

FIG. 3. Phase diagram in the γ-g plane. The dotted line shows the g dependence of γ according to Eq. (19) for $\tilde{\gamma}=0.36$.

large $\tilde{\gamma}$, a nonmagnetic phase emerges. It appears that a broadening of the pseudofermion levels captures much of the effect of frustration expected to reduce or destroy magnetic order. In contrast to the simple mean-field theory, one now finds second-order phase transitions and a mean-field critical exponent $\beta=\frac{1}{2}$ of the magnetization. From the self-consistent equations, a phase diagram in the γ-g plane can be drawn, see Fig. 3. It shows only a narrow parameter range for γ where the theory provides meaningful values for the phase boundaries. For that reason, it will be difficult to determine the damping parameter in approximative schemes. For example, $\tilde{\gamma}=0.36$ leads to transitions at $g_{c1}\approx 0.39$, $g_{c2}\approx 0.69$, and also a realistic value for the magnetization at $g=0$, i.e., $M_{\text{Néel}}\approx 0.35$. This value of the width parameter $\tilde{\gamma}$ will be used in the following section to study the properties of the nonmagnetic phase.

B. Random-phase approximation

In this section, we calculate the spin susceptibility in the paramagnetic phase within RPA using the Green's function introduced in the last section. Figure 4 displays the approximation in diagrammatic form. Since the RPA scheme can be obtained from the Hartree approximation by taking the derivative with respect to the self-consistent field, the quantum phase transitions are located at the same point in both approaches. The conserving approximation scheme in the sense of Baym and Kadanoff[65,66] is an essential aspect here because spin conservation is an important constraint on the dynamics of the physical system; in addition the auxiliary-particle constraint which allows only one particle per site requires a conserved particle number. In the nonmagnetic phase, the equations in Fig. 4 are translation invariant and can be transformed into momentum space. The static susceptibility $\chi(\mathbf{p},i\nu=0)$ then has the form

$$\chi(\mathbf{p},i\nu=0)=\frac{1}{[\Pi(i\nu=0)]^{-1}+J(\mathbf{p})}. \tag{22}$$

Here $J(\mathbf{p})$ is the Fourier transform of the interaction $J_{ij}\equiv J_{i-j}$ which is given by

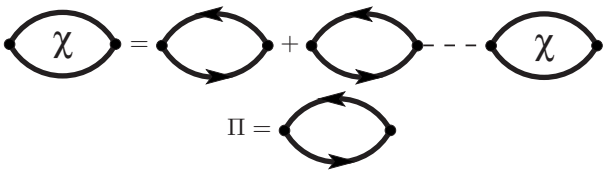

FIG. 4. Self-consistent RPA equation for the susceptibility χ in diagrammatic representation. Π denotes a single bubble.

$$J(\mathbf{p})=2J_1[\cos(p_x)+\cos(p_y)]+4J_2\cos(p_x)\cos(p_y). \tag{23}$$

Inserting the propagator from Eq. (18) into a single bubble $\Pi(i\nu=0)$, this quantity is found as

$$\Pi(i\nu=0)\equiv\Pi^{zz}(i\nu=0)=$$
$$-\frac{1}{4}\frac{1}{2\pi}\int d\omega\left(\frac{1}{i\omega+i\gamma\,\mathrm{sgn}(\omega)}\right)^2\mathrm{Tr}[(\sigma^z)^2]=\frac{1}{2\pi\gamma}. \tag{24}$$

The susceptibility in Eq. (22) together with Eqs. (19), (23), and (24) is evaluated for $\mathbf{p}=(\pi,\pi)$ and $\mathbf{p}=(\pi,0)$, the relevant wave vectors in the case of Néel and Collinear orders, respectively. The results are shown in Fig. 5. As expected for continuous phase transitions, the susceptibility with wave vector $\mathbf{p}=(\pi,\pi)(\mathbf{p}=(0,\pi))$ diverges in the limit $g_c\to g_{c1}+0$ $(g_c\to g_{c2}-0)$.

Finally, we discuss the static correlation function $\chi(\mathbf{R},i\nu=0)$, which is obtained by transforming the susceptibility from Eq. (22) into real space,

$$\chi(\mathbf{R},i\nu=0)=\frac{1}{(2\pi)^2}\int_{-\pi}^{\pi}dp_x\int_{-\pi}^{\pi}dp_y\frac{e^{i\mathbf{pR}}}{[\Pi(i\nu=0)]^{-1}+J(\mathbf{p})}. \tag{25}$$

Evaluating Eq. (25) numerically with $\tilde{\gamma}=0.36$ for distances R along the vertical or horizontal lattice direction, $\mathbf{R}_\mu=R\mathbf{e}_\mu$, $\mu=x,y$, leads to the behavior shown in Fig. 6. For g slightly above the lower critical value g_{c1} (upper panel), the signature

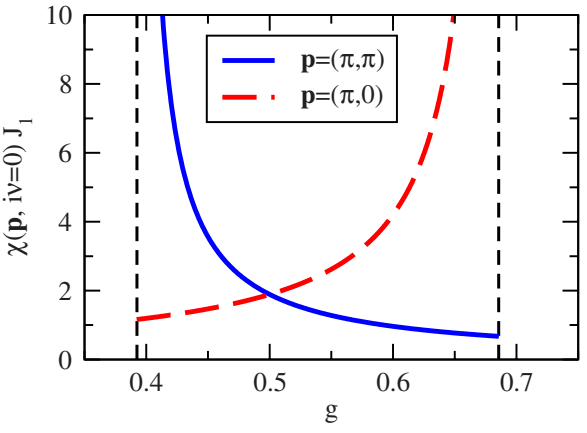

FIG. 5. (Color online) Static susceptibility for wave vectors (π,π) and $(\pi,0)$ and a damping parameter $\tilde{\gamma}=0.36$. The dashed lines visualize the phase boundaries.

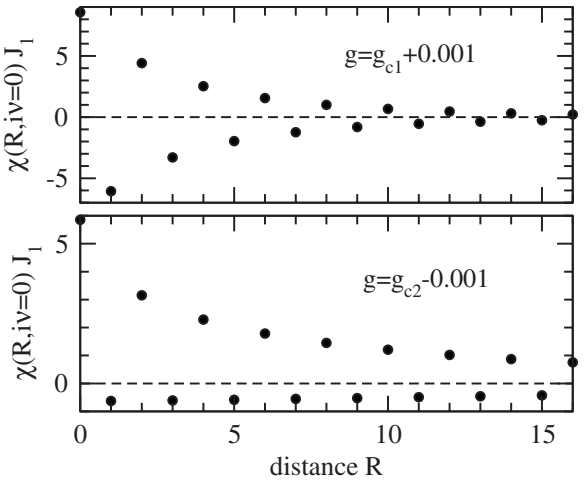

FIG. 6. Static correlation function $\chi(R,i\nu=0)$ for distances $R=|\mathbf{R}|$ along a lattice direction. R is measured in units of a lattice spacing. Again $\tilde{\gamma}=0.36$ is used. In the upper panel, g is slightly above the critical point g_{c1} and in the lower panel slightly below g_{c2}.

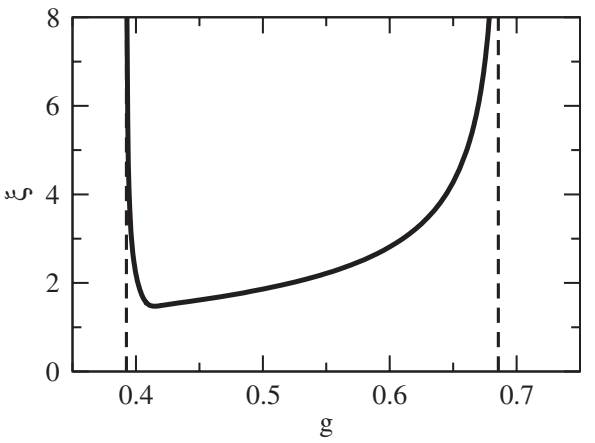

FIG. 7. Static correlation length ξ in units of a lattice spacing versus g. The spectral width is $\tilde{\gamma}=0.36$.

of the Néel phase is clearly seen. The correlation function forms a staggered pattern and the envelopes for positive and negative values only differ by a sign. At large enough distances R, the data points are well fitted by an exponential decay while at small distances, the decrease is faster. Inside the paramagnetic phase, the envelopes are no longer symmetric around $\chi(R)=0$. For g slightly below the upper critical point g_{c2} (lower panel), the correlation function still exhibits a staggered sign but the correlation between spins with an odd distance seems to vanish on approaching the critical point. Again, for large R, an exponential function can be fitted and the correlation length is identical for even and odd distances. The asymmetry of the two envelopes can be understood by the fact that for Collinear fluctuations, two degenerate patterns exist, the alignment of spins along rows and along columns. Thus, near the upper critical point correlations are a superposition of both,

$$\chi(R) = (-1)^R a_1 e^{-R/\xi} + a_2 e^{-R/\xi} \tag{26}$$

with (almost) identical weights $a_1=a_2$. Obviously this suppresses correlations for odd distances. Here ξ denotes the correlation length. Away from the upper critical point Néel-type fluctuations emerge and we have $a_1>a_2$. Eventually at the lower critical point a_2 vanishes.

The correlation length ξ is plotted in Fig. 7. The data indicate divergences at the phase boundaries but get rather small in the vicinity of $g=0.4$, i.e., down to $\xi\approx 1.5$. Remarkably, the smallest values for the correlation length are not reached at $g=0.5$ where one would classically expect the strongest frustration.

The phenomenological theory presented suggests that a broadening of the fermions' spectral function controls the phase diagram and the behavior of many physical quantities such as the magnetization, the susceptibility, and the spatial correlation function. However, a statement about the nature of the paramagnetic phase (columnar dimer or plaquette order) cannot be made. Also critical behavior beyond mean field is not accessible. Qualitatively correct results are obtained by tuning the width $\tilde{\gamma}$. However, this phenomenological parameter is not calculated within the theory and there is no simple way to calculate it. Unfortunately, summing up diagrammatic contributions of the Green's function to gain reasonable values for the width is a difficult task[39,40] because the results strongly depend on the choice of the diagrams. For example, in the approximation of taking the self-energy to second order, one gets a spectral function of the form

$$\rho(\omega) = \frac{1}{2}[\delta(\omega-\Delta)+\delta(\omega+\Delta)]. \tag{27}$$

Then in the whole parameter range $g\geq 0$, the gap Δ turns out to be so large that magnetic order is destroyed. On the other hand, from a completely self-consistent calculation of the second-order self-energy, one finds that the spectral function is too narrow to allow for a paramagnetic phase.

Note that there is no justification for a perturbative treatment in finite order. Instead diagram classes up to infinite order have to be summed. To approach this problem in a more systematic way, we will now use the FRG method.

V. FUNCTIONAL RENORMALIZATION-GROUP METHOD

The FRG method allows to sum up infinite classes of contributions in perturbation theory in a systematic way. So far, this method has been used to describe the weak-coupling regime, e.g., of the Hubbard or the Anderson model. Our model does not have a small coupling constant since there is no kinetic-energy term in a spin Hamiltonian. We nonetheless employ FRG in the usual way of neglecting higher order (three-particle and higher-order) correlation functions. As it turns out that this is not sufficient, we add higher-order correlations in the form of self-energy corrections. Within FRG, one starts with the high-energy sector, where Green's functions and coupling functions are known, and successively adds lower-energy contributions. As a first step, we define the cutoff procedure to be used by the following zero-temperature bare Green's function,

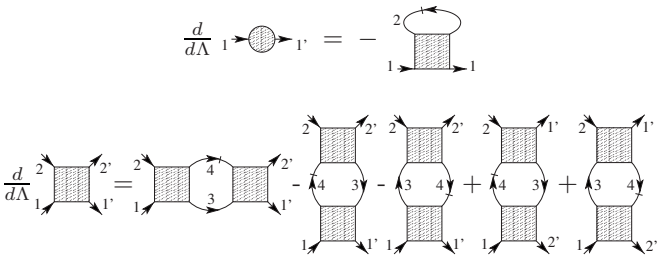

FIG. 8. FRG equations for the self-energy and for the two-particle vertex. The line with an arrow is the full Green's function $G^{\Lambda}(i\omega)$ [see Eq. (31)] and the line with an arrow and a slash is the single-scale propagator $S^{\Lambda}(i\omega)$ [see Eq. (32)].

$$G^{0\Lambda}(i\omega) = \Theta(|\omega| - \Lambda) G^{0}(i\omega) = \frac{\Theta(|\omega| - \Lambda)}{i\omega + \mu}. \tag{28}$$

In this cutoff-dependent propagator, all modes with $|\omega| < \Lambda$ are projected out. For the rest of the paper, we apply the average auxiliary-fermion projection scheme with $\mu = 0$, as it is exact at zero temperature. However, it is not too difficult to implement the exact projection scheme,[54] which increases the numerical effort by roughly a factor of 8. In the one-particle irreducible (1PI) version of FRG (Refs. 57–60) employed here, $G^{0\Lambda}(i\omega)$ is inserted into the generating functional of the 1PI vertex functions[52]in place of $G^{0}(i\omega)$. Taking the derivative with respect to Λ, an exact, infinite hierarchy of coupled differential equations for the vertex functions is obtained. To be more precise, the flow of the one-particle vertex, the self-energy Σ, depends on Σ and the two-particle vertex Γ. In turn, the flow of Γ depends on Σ, Γ, and the three-particle vertex Γ_3, and so on. At the end of the flow at $\Lambda = 0$ when the theory is cutoff free, the exact vertex functions are obtained.[59,60] However, in explicit calculations one can only deal with a finite set of equations and hence a truncation scheme has to be applied. Usually, by applying a weak-coupling approximation, the three-particle vertex Γ_3 and higher vertices are neglected, resulting in a closed set of equations for Σ and Γ. This scheme will be applied in Secs. V A and V B while in Secs. V C and V D, we make use of an improved truncation scheme,[37] which takes into account contributions of the three-particle type. For the conventional truncation scheme, the equations for the self-energy Σ and the two-particle vertex Γ are depicted in Fig. 8. In explicit form, these equations read

$$\frac{d}{d\Lambda}\Sigma^{\Lambda}(1) = -\frac{1}{2\pi}\sum_{2} \Gamma^{\Lambda}(1,2;1,2) S^{\Lambda}(\omega_2), \tag{29}$$

$$\begin{aligned}\frac{d}{d\Lambda}\Gamma^{\Lambda}(1',2';1,2) = \frac{1}{2\pi}\sum_{3,4} [&\Gamma^{\Lambda}(1',2';3,4)\Gamma^{\Lambda}(3,4;1,2) \\ &- \Gamma^{\Lambda}(1',4;1,3)\Gamma^{\Lambda}(3,2';4,2) - (3 \leftrightarrow 4) \\ &+ \Gamma^{\Lambda}(2',4;1,3)\Gamma^{\Lambda}(3,1';4,2) + (3 \leftrightarrow 4)] \\ &\times G^{\Lambda}(\omega_3) S^{\Lambda}(\omega_4).\end{aligned} \tag{30}$$

Here the numbers are shorthand notations for the frequency, the site index, and the spin index, that is, $1 = \{\omega_1, i_1, \alpha_1\}$, and Σ_1 stands for an integral over ω_1 and sums over i_1 and α_1. The full propagator $G^{\Lambda}(i\omega)$ reads

$$G^{\Lambda}(i\omega) = \frac{\Theta(|\omega| - \Lambda)}{i\omega - \Sigma^{\Lambda}(i\omega)} \tag{31}$$

and the so-called single-scale propagator is defined by

$$S^{\Lambda}(i\omega) = [G^{\Lambda}(i\omega)]^2 \frac{d}{d\Lambda}[G^{0\Lambda}(i\omega)]^{-1} = \frac{\delta(|\omega| - \Lambda)}{i\omega - \Sigma^{\Lambda}(i\omega)}. \tag{32}$$

For the last expression in this equation, a relationship[67] for the product of Θ functions and δ functions has been used. Note that G^{Λ} and S^{Λ} are local and translation invariant in real space and proportional to the unit matrix in spin space. Thus, the propagators in Fig. 8 and Eqs. (29) and (30) carry only one composite index.

Next we specify the initial conditions for the flow equations at $\Lambda = \infty$. In this limit, the free propagator vanishes identically. Thus, only one-particle potentials for the self-energy and bare interactions for the two-particle vertex remain. In the following, we confine ourselves to the nonmagnetic phase. We defer consideration of the flow of the magnetic order parameter to later work. Accordingly the free Green's function [Eq. (28)] does not contain a one-particle field m that breaks rotational symmetry as in Eqs. (6) and (8). Note that although within this scheme, the magnetic phases are not accessible, magnetic instabilities may be detected as divergences in the susceptibilities. We have a vanishing self-energy for $\Lambda = \infty$,

$$\Sigma^{\Lambda=\infty}(i\omega) \equiv 0. \tag{33}$$

In this limit, the two-particle vertex is given by the bare interactions in antisymmetrized form,

$$\begin{aligned}\Gamma^{\Lambda=\infty}(1',2';1,2) = &J_{i_1 i_2}\frac{1}{2}\sigma^{\mu}_{\alpha_1'\alpha_1}\frac{1}{2}\sigma^{\mu}_{\alpha_2'\alpha_2}\delta_{i_1' i_1}\delta_{i_2' i_2} \\ &- J_{i_1 i_2}\frac{1}{2}\sigma^{\mu}_{\alpha_1'\alpha_2}\frac{1}{2}\sigma^{\mu}_{\alpha_2'\alpha_1}\delta_{i_1' i_2}\delta_{i_2' i_1}.\end{aligned} \tag{34}$$

Here the factors $\frac{1}{2}\sigma^{\mu}_{\alpha\beta}$ originate from the bare vertices and the Kronecker δ ensures that there is no fermion hopping on the lattice. Since the rotational invariance of the initial conditions is conserved during the flow, the two-particle vertex at finite Λ is parametrized by spin-interaction terms $\propto \sigma^{\mu}_{\alpha\beta}\sigma^{\mu}_{\gamma\delta}$ and density-interaction terms $\propto \delta_{\alpha\beta}\delta_{\gamma\delta}$. Since the propagators are local, the site index of an ingoing leg has to be identical to the site index of the corresponding outgoing leg, which results in a total dependence on only two sites, i.e., i_1 and i_2. To be more precise, translation invariance further reduces the site dependence only to the separation $|i_1 - i_2|$. Taking into account the antisymmetry in all variables, the two-particle vertex can now be represented as

$$\Gamma^{\Lambda}(1',2';1,2) = [\Gamma^{\Lambda}_{\mathrm{s}\,i_1 i_2}(\omega_{1'},\omega_{2'};\omega_1,\omega_2)\sigma^{\mu}_{\alpha_{1'}\alpha_1}\sigma^{\mu}_{\alpha_{2'}\alpha_2} + \Gamma^{\Lambda}_{\mathrm{d}\,i_1 i_2}(\omega_{1'},\omega_{2'};\omega_1,\omega_2)\delta_{\alpha_{1'}\alpha_1}\delta_{\alpha_{2'}\alpha_2}]\delta_{i_{1'}i_1}\delta_{i_{2'}i_2}$$
$$- [\Gamma^{\Lambda}_{\mathrm{s}\,i_1 i_2}(\omega_{1'},\omega_{2'};\omega_2,\omega_1)\sigma^{\mu}_{\alpha_{1'}\alpha_2}\sigma^{\mu}_{\alpha_{2'}\alpha_1} + \Gamma^{\Lambda}_{\mathrm{d}\,i_1 i_2}(\omega_{1'},\omega_{2'};\omega_2,\omega_1)\delta_{\alpha_{1'}\alpha_2}\delta_{\alpha_{2'}\alpha_1}]\delta_{i_{1'}i_2}\delta_{i_{2'}i_1}. \quad (35)$$

The indices s/d correspond to spin and density interactions. Note that energy conservation is implied, i.e., $\omega_{1'}+\omega_{2'}=\omega_1+\omega_2$. As another consequence of rotational invariance, the self-energy is an odd function in the frequency, as already pointed out after Eq. (17). In analogy to Eq. (17), we write

$$\Sigma^{\Lambda}(i\omega) = -i\gamma^{\Lambda}(\omega). \quad (36)$$

Inserting Eqs. (31), (32), (35), and (36) into Eqs. (29) and (30), the flow equations for γ, Γ_{s}, and Γ_{d} can be calculated.

A. Static FRG

Before considering the general case with all frequency dependencies, in this section we briefly discuss a static approximation.[63,68] Putting all frequency arguments of the self-energy and vertex functions equal to zero leads, however, to a trivial solution since in that case, the self-energy will be identically zero, provided it is assumed to be a continuous function of frequency. Therefore, in order to allow for a broadening of the spectrum we again assume the discontinuous form $\Sigma^{\Lambda}=-i\gamma^{\Lambda}\,\mathrm{sgn}(\omega)$. However, inserting this form together with the static two-particle vertex into the first flow Eq. (29) leads to a vanishing flow for γ^{Λ} due to the integration over an odd function on the right side. Obviously a static approximation can only be applied to the two-particle vertex, and γ^{Λ} has to be considered again as a phenomenological parameter that is independent of Λ. Using the static version of Eq. (35), i.e.,

$$\Gamma^{\Lambda}(1',2';1,2) = [\Gamma^{\Lambda}_{\mathrm{s}\,i_1 i_2}\sigma^{\mu}_{\alpha_{1'}\alpha_1}\sigma^{\mu}_{\alpha_{2'}\alpha_2} + \Gamma^{\Lambda}_{\mathrm{d}\,i_1 i_2}\delta_{\alpha_{1'}\alpha_1}\delta_{\alpha_{2'}\alpha_2}]\delta_{i_{1'}i_1}\delta_{i_{2'}i_2}$$
$$- [\Gamma^{\Lambda}_{\mathrm{s}\,i_1 i_2}\sigma^{\mu}_{\alpha_{1'}\alpha_2}\sigma^{\mu}_{\alpha_{2'}\alpha_1} + \Gamma^{\Lambda}_{\mathrm{d}\,i_1 i_2}\delta_{\alpha_{1'}\alpha_2}\delta_{\alpha_{2'}\alpha_1}]\delta_{i_{1'}i_2}\delta_{i_{2'}i_1} \quad (37)$$

and the phenomenological assumption $\Sigma(i\omega)=-i\gamma\,\mathrm{sgn}(\omega)$, one obtains

$$\frac{d}{d\Lambda}\Gamma^{\Lambda}_{\mathrm{s}\,i_1 i_2} = \frac{2}{\pi}\frac{1}{(\Lambda+\gamma)^2}\Bigg[\sum_j \Gamma^{\Lambda}_{\mathrm{s}\,i_1 j}\Gamma^{\Lambda}_{\mathrm{s}\,j i_2} - 2(\Gamma^{\Lambda}_{\mathrm{s}\,i_1 i_2})^2 + \Gamma^{\Lambda}_{\mathrm{s}\,i_1 i_2}(\Gamma^{\Lambda}_{\mathrm{s}\,i_1 i_1} - \Gamma^{\Lambda}_{\mathrm{d}\,i_1 i_1})\Bigg], \quad (38a)$$

$$\frac{d}{d\Lambda}\Gamma^{\Lambda}_{\mathrm{d}\,i_1 i_2} = \frac{2}{\pi}\frac{1}{(\Lambda+\gamma)^2}\Bigg[\sum_j \Gamma^{\Lambda}_{\mathrm{d}\,i_1 j}\Gamma^{\Lambda}_{\mathrm{d}\,j i_2} - \Gamma^{\Lambda}_{\mathrm{d}\,i_1 i_2}(3\Gamma^{\Lambda}_{\mathrm{s}\,i_1 i_1} + \Gamma^{\Lambda}_{\mathrm{d}\,i_1 i_1})\Bigg]. \quad (38b)$$

Note that the frequency dependence of Σ only affects the internal integration. By comparing Eqs. (34) and (37), the initial conditions for Γ_{s} and Γ_{d} can be read off,

$$\Gamma^{\Lambda=\infty}_{\mathrm{s}\,i_1 i_2} = \frac{1}{4}J_{i_1 i_2}, \quad (39a)$$

$$\Gamma^{\Lambda=\infty}_{\mathrm{d}\,i_1 i_2} = 0. \quad (39b)$$

Solving Eq. (38b) with the initial condition (39b) gives $\Gamma^{\Lambda}_{\mathrm{d}\,i_1 i_2}\equiv 0$. A finite set of equations for $\Gamma^{\Lambda}_{\mathrm{s}\,i_1 i_2}$ is obtained by neglecting all vertices with the distance $|i_1-i_2|$ exceeding a certain cutoff value. The resulting equations are solved numerically. A flow toward finite values for $\Lambda\to 0$ indicates a paramagnetic phase while a diverging flow is a sign of a magnetic instability. The type of order can be extracted by transforming $\Gamma^{\Lambda}_{\mathrm{s}\,i_1 i_2}$ into Fourier space and identifying the fastest momentum component. As a result, one can draw a phase diagram in the γ-g plane, see Fig. 9. The figure compares the phase boundaries with the results from the phenomenological theory in Sec. IV. Again the boundaries are given by straight lines but the value of the frustration parameter for which the paramagnetic phase has its largest extent moved from $g=0.5$ to $g\approx 0.62$. Interestingly, the phase diagram from Sec. IV can be reproduced within FRG. Consider the flow equation depicted in Fig. 10. It only contains the second and third term of the right side of the equation in Fig. 8. Furthermore, it specifies how the ingoing and the outgoing lines are connected. An examination of the terms in Fig. 8 reveals that the contributions in Fig. 10 are the only ones that couple two-particle vertices with different spatial separations of the outer legs among each other. This is due to the internal fermion bubbles in Fig. 10 which can be located on an arbitrary site. For the other terms, the vertex on the left side of

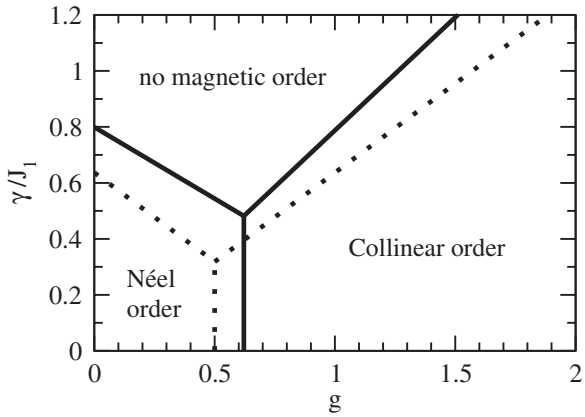

FIG. 9. Phase diagram in the γ-g plane for a static FRG approximation including a phenomenological parameter γ (full line). The dotted line shows the phase boundaries of the phenomenological theory from Fig. 3.

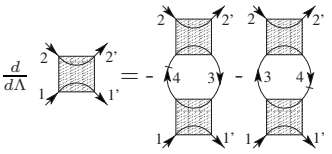

FIG. 10. FRG equation for the RPA scheme. The lines inside the boxes indicate the connections of the external legs.

the flow equation is coupled only to itself or to the local vertex. The explicit equation corresponding to Fig. 10 reads

$$\frac{d}{d\Lambda}\Gamma^{\Lambda}_{\mathrm{s}i_1i_2} = \frac{2}{\pi}\frac{1}{(\Lambda+\gamma)^2}\sum_j \Gamma^{\Lambda}_{\mathrm{s}i_1j}\Gamma^{\Lambda}_{\mathrm{s}ji_2}, \tag{40}$$

again with a phenomenological γ. It can be shown[38] that Eq. (40) reproduces the static RPA scheme and the phase diagram of Sec. IV. Evidently the terms in Fig. 10 are essential to obtain magnetism since they are the only ones that are able to describe collective phenomena. On the other hand, the remaining terms in Fig. 8 are only corrections that do not modify the phase diagram qualitatively.

B. Dynamic FRG

The considerations in Sec. V B led to the conclusion that a static approximation of the FRG equations does not allow to calculate the central quantity governing the destruction of long-range order: the pseudofermion spectral width γ. We will now treat the FRG equations in its full complexity and consider the dynamics with all frequency dependences as well as the back coupling of the self-energy into the two-particle vertex. This will lead to a finite spectral broadening without further assumptions. Again we make use of the truncation scheme that omits all vertices higher than the two-particle vertex. Inserting Eqs. (31), (32), (35), and (36) into Eqs. (29) and (30), after a lengthy but straightforward calculation we end up with the flow equations and initial conditions presented in the Appendix. For convenience, we write the two-particle vertex as a function of the invariant frequency variables s, t, and u,

$$\Gamma^{\Lambda}_{\mathrm{s/d}\,i_1i_2}(\omega_{1'},\omega_{2'};\omega_1,\omega_2) \to \Gamma^{\Lambda}_{\mathrm{s/d}\,i_1i_2}(s,t,u), \tag{41}$$

defined by $s=\omega_1+\omega_2$, $t=\omega_{1'}-\omega_1$, and $u=\omega_{1'}-\omega_2$. The advantage of this parametrization is that Γ_{s} and Γ_{d} are both invariant under each of the transformations $s\to -s$, $t\to -t$, and $u\to -u$, which can be deduced by a careful examination of the flow equations. This simplifies the numerics since only positive s, t, and u have to be considered.

In order to solve these equations numerically, the continuous frequencies will be discretized. We use a combination of a linear and a logarithmic mesh. Since the two-particle vertex depends on three frequencies, the computational effort grows with the third power of the number of discrete frequencies. Regarding the truncation in real space, the computing time grows with the fourth power of the length of the longest two-particle vertex [in two dimensions, counting an internal site summation, see Eqs. (A2) and (A3)].

From the numerical solution, we obtain physical quantities such as the static correlation function $\chi_{ij}(i\nu=0)$ by connecting the fermion lines of the two-particle vertex,

$$\chi_{ij}(i\nu=0) = \int_0^\infty \mathrm{d}\tau \left\langle T_\tau \left\{ S_i^z(\tau) S_j^z(0) \right\} \right\rangle$$

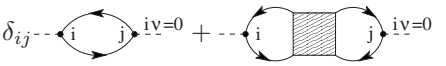

(42)

To calculate this diagram two frequency integrals have to be performed numerically. The physical correlation function is recovered in the limit $\Lambda=0$ but we also consider χ_{ij} at finite Λ. Transforming χ^{Λ}_{ij} into momentum space, we obtain the magnetic susceptibility $\chi^{\Lambda}(\mathbf{p})$. The results are plotted in Figs. 11 and 12. It is seen that during the flow the Néelsusceptibility [$\mathbf{p}=(\pi,\pi)$] exhibits a divergence for all $g\lesssim 0.55$. On the other hand, the Collinear susceptibility appears to diverge for all $g\gtrsim 0.55$. In particular, there is no parameter region without a magnetic instability and with a flow down to $\Lambda=0$. In the present approximation, the paramagnetic phase is obviously missing. The abrupt stop of the flow of the susceptibilities for $g\gtrsim 0.6$ in Fig. 11 and $g\lesssim 0.55$ in Fig. 12 can be traced to the divergence of the respective other susceptibility. For g at the transition, i.e., between 0.55 and

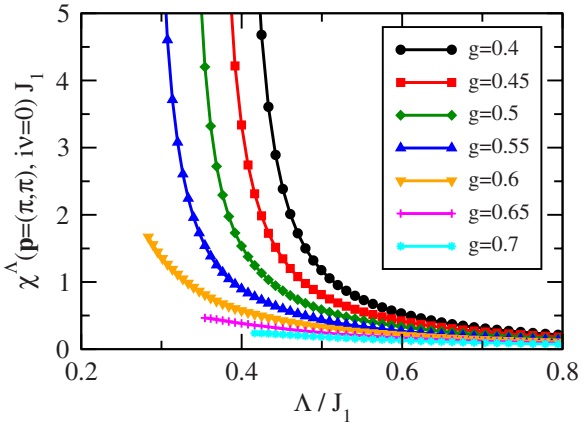

FIG. 11. (Color online) Flow of the static Néel susceptibility for different frustrations.

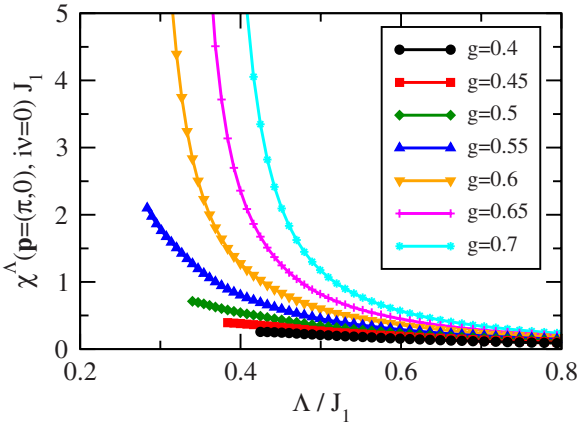

FIG. 12. (Color online) Flow of the static Collinear susceptibility for different frustrations.

0.6, the divergence is clearly indicated at the smallest accessible Λ.

The absence of a nonmagnetic phase is quite unsatisfactory. Obviously the spectral width comes out too small in this approximation. However, an essential improvement is made in the next section where we use a different truncation scheme.

C. Katanin truncation

The only approximation that is involved in the FRG scheme described above is the truncation procedure in the hierarchy of differential equations. Unfortunately, the simple truncation employed above violates conservation laws, expressed in terms of Ward identities. In order to improve the fulfillment of Ward identities, Katanin developed a one-particle self-consistent version of the two-loop FRG equations.[37] The basic modification there is the substitution of the single-scale propagator S^Λ, see Eq. (32), by the total derivative of $-G^\Lambda$ with respect to Λ,

$$S^\Lambda(i\omega) \to -\frac{d}{d\Lambda}G^\Lambda(i\omega) = S^\Lambda(i\omega) - [G^\Lambda(i\omega)]^2\frac{d}{d\Lambda}\Sigma^\Lambda(i\omega). \tag{43}$$

It can be shown[37,38] that such an approach is equivalent to an RPA+Hartree approximation if only terms of the RPA type (Fig. 10) are kept in the flow equation for the two-particle vertex. In this case, Ward identities generated by spin conservation are fulfilled exactly. As an application in a different context, for the reduced BCS model of superconductors exact mean-field results have been reproduced.[38] In particular, in conjunction with a small symmetry-breaking external field this scheme allows to access symmetry-broken phases.[38,69,70] If one keeps the terms additional to RPA on the right-hand side of the second flow equation (see Fig. 8 and also Ref. 60), as we do, the exact conservation property is lost but the remaining symmetry violating terms are generated by overlapping loop diagrams and may be expected to be smaller (see Ref. 37). While on the one hand, the Katanin truncation scheme assures that the terms of an RPA+Hartree resummation are correctly included, we find that the non-RPA terms are essential in providing just the right size of a finite auxiliary-particle spectral linewidth. In that sense, the non-RPA terms play a crucial role here: they control the pseudofermion damping and therefore the size of the nonmagnetic region in the phase diagram.

As described in Ref. 38 the substitution [Eq. (43)] is made in Eq. (30) but not in the equation, for the self-energy, Eq. (29). In the present work, the above-mentioned small symmetry-breaking field is not applied. This would break the invariance of the two-particle vertex under $s \to -s$, $t \to -t$, and $u \to -u$ and would generate additional terms in the spin parametrization [Eq. (35)]. Effectively, with the substitution [Eq. (43)] also contributions from the three-particle vertex are included. In the numerical implementation, in the equations for the two-particle vertex the internal bubble $P^\Lambda_{\rm con}$, Eq. (A5), is replaced by the modified bubble $P^\Lambda_{\rm Kat}$, Eq. (A6). Due to the last term in Eq. (A6) which does not contain a δ function, the internal frequency integration has to be performed explicitly. As a result, now the computing time grows with the fourth power of the number of discrete frequencies.

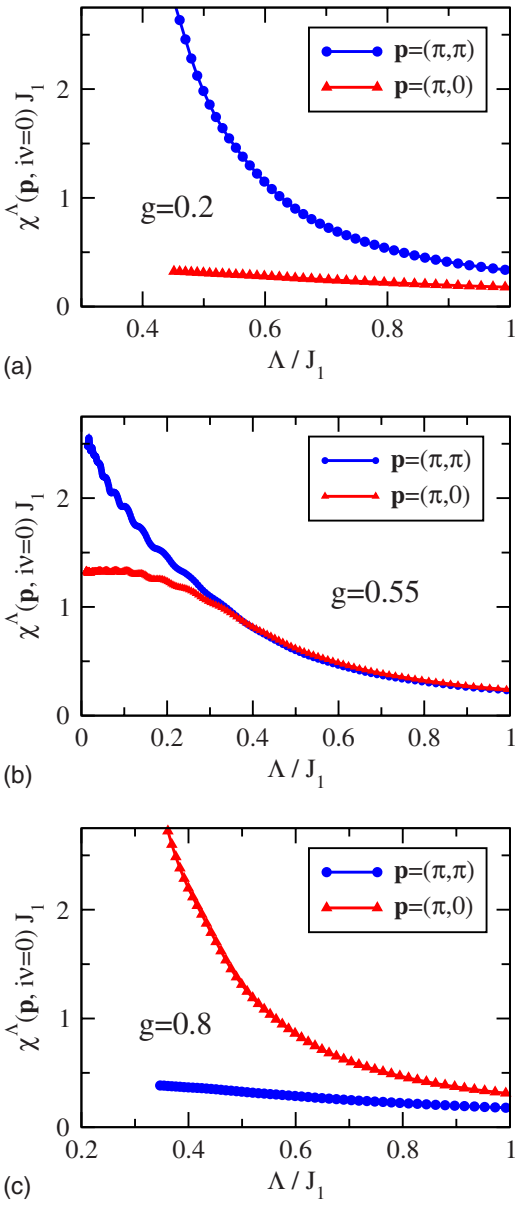

FIG. 13. (Color online) Flow of the static susceptibility for the wave vectors $\mathbf{p}=(\pi,\pi)$ and $\mathbf{p}=(\pi,0)$ and different parameters g, (a) $g=0.2$, (b) $g=0.55$, and (c) $g=0.8$.

Typically we use 64 frequencies and discard all two-particle vertices with a spatial extent larger than seven lattice spacings in each direction. Note that this truncation corresponds to a system with 14×14 sites and periodic boundary conditions because the longest bond in such a system extends over 7×7 sites. Exploiting lattice symmetries we end up with approximately $2.5\cdot10^6$ coupled differential equations. The numerically determined coupling functions and self-energies are inserted into Eq. (42) to calculate the susceptibilities shown in Fig. 13. In the course of the flow, the Néel susceptibility for $g=0.2$ shows a pronounced increase while the Collinear one stays very small, see Fig. 13(a). Obviously at that degree of frustration, the system is in the Néel phase. However, we do not observe a real divergence of the suscep-

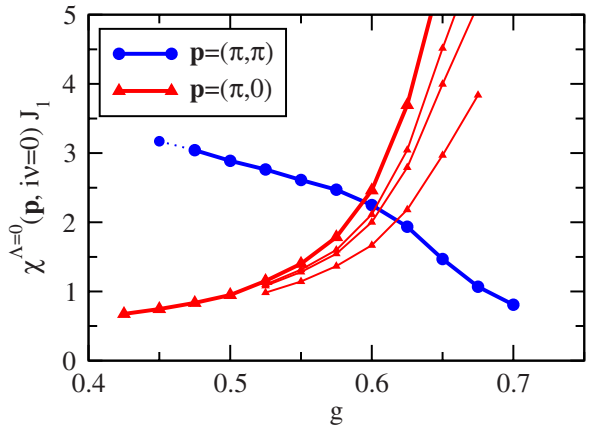

FIG. 14. (Color online) Static susceptibility for the paramagnetic phase in the physical limit $\Lambda=0$. The thick lines are obtained by a finite-size scaling. The thin lines are the results for a maximal bond length of 7×7, 5×5, and 3×3 sites, from top to bottom.

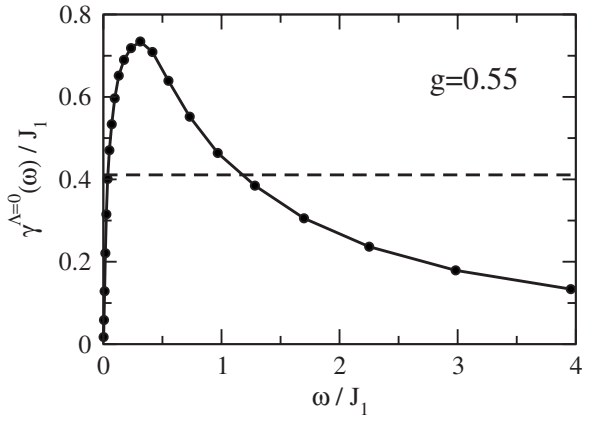

FIG. 15. Frequency-dependent damping $\gamma^{\Lambda=0}(\omega)$ obtained at the end of the FRG flow compared to the constant damping with $\tilde{\gamma}=0.36$ used in Sec. IV (dashed line). Depicted is the case $g=0.55$.

tibility. When Λ gets too small, the increase in the susceptibility stops and the flow exhibits an unstable and wiggly behavior which we attribute to numerical instabilities. Especially, for small Λ, the flow is sensitive to the discretization of the frequencies. Going to larger system sizes, the situation improves, i.e., one can follow the flow to larger susceptibilities and finds a steeper increase. Thus, unstable flows at small Λ can be identified as finite-size effects. In the thermodynamic limit and with a sufficient number of discrete frequencies, we expect a smooth, diverging solution indicating a magnetic instability.

At $g=0.55$, see Fig. 13(b), both susceptibilities approach finite values for $\Lambda\to0$, demonstrating the existence of a phase with neither Néel nor Collinear long-range order. Small oscillations are a consequence of the frequency mesh. In our numerics, the limit $\Lambda=0$ cannot be reached exactly because of an insufficient number of discrete frequencies at very low-energy scales. Typically the flow is stopped at $\Lambda\approx0.01\ J_1$ but can be easily extrapolated to $\Lambda=0$. Finally at $g=0.8$ the Collinear phase can be identified. In Fig. 13(c), the behavior is analogous to Fig. 13(a) but showing an increasing Collinear susceptibility.

In order to investigate the properties of this phase further, we calculated the susceptibilities at additional parameter values. The results in the physical limit $\Lambda=0$ are shown in Fig. 14. Deep inside the paramagnetic phase our results are well converged. With increasing g, we observe a decreasing Néel susceptibility and an increasing Collinear susceptibility. The point where Néel-type fluctuations loose out compared to Collinear fluctuations lies at $g\approx0.6$ in correspondence with the results in Sec. V A, i.e., clearly higher than the classical value $g=0.5$. At the phase boundary to Collinear order, which turns out to be in the range $g_{c2}\approx0.66\ldots0.68$, the critical fluctuations require large system sizes, in order to obtain well-converged results. Here a finite-size scaling (see thin lines in Fig. 14) considerably enhances the Collinear susceptibility and a beginning divergence is visible. The situation is very different near the phase boundary to Néel order. A divergence of the Néel susceptibility is not seen and finite-size effects play a minor role. Instead, here the flow is highly sensitive to the frequency discretization, which causes large oscillations. Therefore, it seems to be difficult to access this critical region and to obtain reliable data, see the dotted part of the blue line in Fig. 14. Here a denser mesh enhances and smooths the Néel susceptibility during the flow. An estimation of this phase boundary leads to the parameter region $g_{c1}\approx0.4\ldots0.45$.

Only few results on spin susceptibilities are found in the literature.[18] To the best of our knowledge, so far no data are available for static spin susceptibilities. We note that our results on the phase boundaries are in good agreement with previous results.[18,20,21,28,44,46]

So far we notice that the behavior of the system near the two transitions is very different. To draw a conclusion concerning the order of the transitions, a closer investigation taking into account a flowing order parameter is necessary.

Although the tendency toward formation of Néel and Collinear phases has already been seen in the standard truncation of the previous section, the inclusion of certain higher-order terms turns out to be essential. As shown above, the non-RPA-like terms in conjunction with the Katanin truncation indeed lead to a damping $\gamma^{\Lambda}(\omega)$ which is strong enough to generate a nonmagnetic phase. The damping which is related to the self-energy via Eq. (36) is no physical observable. This quantity is obtained from the first flow equation and can be compared with the frequency independent γ used in the phenomenological theory from Sec. IV, see Fig. 15. At $g=0.55$, i.e., in the nonmagnetic region we find that $\gamma^{\Lambda=0}(\omega)$ compares quite well with the choice $\tilde{\gamma}=0.36$ in Eq. (19) at relevant energy scales $\omega\sim J$. In the region with high frustration, $g\approx0.55$, the static two-particle vertex $\Gamma^{\Lambda}_{s i_1 i_2}(s=0,t=0,u=0)$, where i_1 and i_2 are nearest neighbors and using the initial conditions given by Eq. (A7), comes out as $\Gamma^{\Lambda=0}_{s i_1 i_2}(0,0,0)\approx1.8\ J_1$ at the end of the flow.

D. Columnar dimer and plaquette order

In this section, we discuss the nature of the paramagnetic phase and investigate whether there is still some kind of long-range order. Possible states currently under discussion

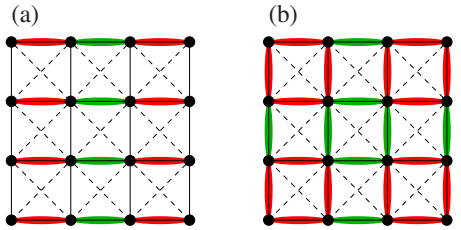

FIG. 16. (Color online) Patterns for (a) columnar dimerization and (b) plaquette dimerization. The two types of bonds correspond to strengthened and weakened interactions in the Hamiltonian $H+F_{\mathrm{d}}$ or $H+F_{\mathrm{p}}$.

are a spin-liquid state (which does not break any symmetries) and a VBS state. For the VBS, two dimerization patterns are of special interest. In a columnar dimer arrangement translation invariance along one lattice direction as well as rotation symmetry are broken. For a plaquette valence-bond ordering, translation symmetry in both directions is broken while the rotation symmetry is intact.

In order to probe the paramagnetic phase with respect to these states, we add a small perturbation field to the Hamiltonian and investigate the response to it.[19–21,23,28,29,47] In the context of FRG, this concept has already been applied in Refs. 38 and 69. The fields can be chosen as

$$F_{\mathrm{d}} = \delta \sum_{i,j} (-1)^i \mathbf{S}_{i,j}\mathbf{S}_{i+1,j},$$

$$F_{\mathrm{p}} = \delta \sum_{i,j} [(-1)^i \mathbf{S}_{i,j}\mathbf{S}_{i+1,j} + (-1)^j \mathbf{S}_{i,j}\mathbf{S}_{i,j+1}], \tag{44}$$

for the columnar dimer and plaquette orders, respectively. Here i and j are components of the position vector and δ is an energy much smaller than J_1 and J_2. Note that the expectation values $\langle F_{\mathrm{d}}\rangle$ and $\langle F_{\mathrm{p}}\rangle$ are the order parameters of these states. F_{d} (see Refs. 19–21, 23, 28, 29, and 47) and F_{p} (see Refs. 20 and 21) break the above-mentioned lattice symmetries and generate the two dimerization patterns shown in Fig. 16. Possible instabilities should be visible as divergences in the corresponding equal time-correlation functions $\chi_{\mathrm{d/p}} = \frac{d\langle F_{\mathrm{d/p}}\rangle}{d\delta}\big|_{\delta=0}$.

The coupling to these operators is included in the FRG formalism by modifying the initial conditions. The bare interactions in the limit $\Lambda \to \infty$ are slightly strengthened or weakened according to the dimerization patterns. Furthermore, we have to take into account that due to the broken translation symmetries a two-particle vertex is no longer uniquely determined by one lattice vector. In the course of the flow, we calculate the correlations of strengthened and weakened bonds and its relative difference. We define equal-time dimer and plaquette correlation functions by

$$\chi^{\Lambda}_{\mathrm{d/p}} = \frac{J_1}{\delta} \frac{|\langle\langle \mathbf{S}_{i,j},\mathbf{S}_{i+1,j}\rangle\rangle^{\Lambda}_{\mathrm{d/p}} - \langle\langle \mathbf{S}_{i+1,j},\mathbf{S}_{i+2,j}\rangle\rangle^{\Lambda}_{\mathrm{d/p}}|}{(\langle\langle \mathbf{S}_{i,j},\mathbf{S}_{i+1,j}\rangle\rangle^{\Lambda}_{\mathrm{d/p}} + \langle\langle \mathbf{S}_{i+1,j},\mathbf{S}_{i+2,j}\rangle\rangle^{\Lambda}_{\mathrm{d/p}})}. \tag{45}$$

Here the index d/p indicates that the correlator $\langle\langle\cdots\rangle\rangle$ is calculated with the Hamiltonian $H+F_{\mathrm{d/p}}$. The factor δ in the denominator eliminates the dependence on the strength of the perturbation such that $\chi^{\Lambda}_{\mathrm{d/p}}$ start with the initial value

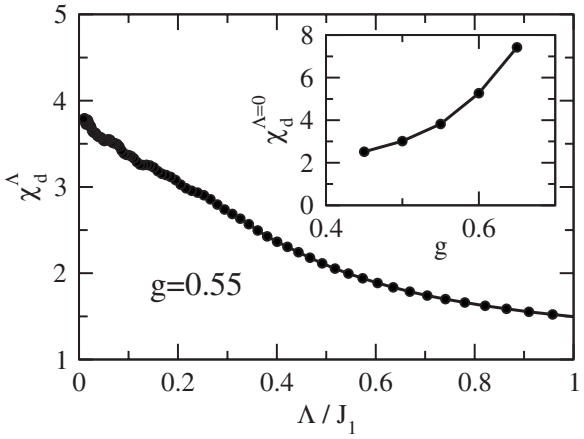

FIG. 17. Main figure: flowing dimer correlation $\chi^{\Lambda}_{\mathrm{d}}$ for $g=0.55$. Inset: dimer correlation $\chi^{\Lambda=0}_{\mathrm{d}}$ in the limit $\Lambda=0$ versus g.

$\chi^{\Lambda=\infty}_{\mathrm{d/p}}=1$. An increase (decrease) during the flow shows that the system supports (rejects) the perturbation. Note that we again apply Katanin's truncation scheme.

The columnar dimer correlation $\chi^{\Lambda}_{\mathrm{d}}$ is plotted in Fig. 17. It is seen that this quantity increases considerably during the flow. In the limit $\Lambda=0$, the perturbation is enhanced by a factor of ≈ 3.8 but a divergence does not occur. We do not exclude an instability for this kind of order which might be masked here due to finite-size effects. Remarkably we obtain plaquette correlations $\chi^{\Lambda}_{\mathrm{p}}$ with the same strength. Apparently the FRG scheme is not able to distinguish between dimer and plaquette correlations. This might be a consequence of the fact that the four-particle vertex from which such susceptibilities can be calculated directly, is not included in our FRG equations. The oscillations during the flow are again a consequence of the frequency mesh.

Thus, our results favor a spin liquid with enhanced equal time correlations χ_{d}, χ_{p} or a VBS with one of the two arrangements. Previous papers mainly calculated the columnar dimer and plaquette susceptibilities in the magnetically ordered phases rather than in the paramagnetic phase.[19,20,28,29]

VI. SUMMARY

The aim of this work is the development of new methods and the calculation of properties for frustrated quantum spin models. We focused on the spin-1/2 J_1-J_2 Heisenberg antiferromagnet on the square lattice but our method is generally applicable to models of that type. Starting point of our approach is perturbation theory in the exchange couplings, summed to infinite order. In order to be able to use standard many-body techniques and to perform diagrammatic expansions, we applied the auxiliary-fermion representation of spin operators. To enforce the auxiliary-particle constraint, two different projection schemes have been employed: (1) enforcement of the constraint on the average (which, however, becomes exact at zero temperature) and (2) exact projection using an imaginary chemical potential.[54]

In a first exploratory study, we use the RPA+Hartree approximation to access the ground-state properties. Since the straightforward mean-field approach is not able to describe

the suppression of magnetic order near $g=\frac{J_2}{J_1}=0.5$, we introduce a damping term in the bare pseudofermion Green's function. This phenomenological self-energy accounts for scattering processes of the auxiliary fermions which lead to a finite lifetime and a spectral broadening. We show that the damping reduces the magnetic order especially in the regime of strong frustration. For sufficiently large damping, one finds a paramagnetic phase around $g=\frac{J_2}{J_1}=0.5$, as seen in numerical studies (we term this phase paramagnetic although it may possess more complex magnetic correlations). Furthermore, using RPA, we calculate the magnetic susceptibility and the spin correlations in the nonmagnetic phase. We observe critical behavior at the phase boundaries, i.e., a divergent susceptibility and correlation length. Within this method, the basic properties come out qualitatively well but a microscopic derivation of the pseudofermion damping is beyond the reach of simple diagrammatic resummations.

A more systematic approach is considered in the main part of the paper: the FRG method. We employ its formulation in terms of the one-particle irreducible vertex functions and use a sharp frequency cutoff Λ. This method sums up large diagram classes in a systematic way, e.g., the two-particle vertex function in the particle-particle channel and in two particle-hole channels and reaches therefore far beyond the mean-field theory. Self-energy contributions are taken into account on equal footing with the vertex renormalizations.

First we apply the conventional truncation scheme to the hierarchy of FRG differential equations, neglecting all vertices higher than the two-particle vertex. Further imposing the static approximation, we find that the pseudofermion broadening is not generated in this way. Adding a phenomenological broadening, the results of the phenomenological theory are recovered, which is saying that RPA-like diagrams in the particle-hole channel can be identified as the most important contributions. Including the frequency dependencies of the self-energy and the two-particle vertex, we find magnetic instabilities in the whole parameter range. The latter is signaled by an immanent divergence of the susceptibilities at $\mathbf{p}=(\pi,\pi)$ and/or $\mathbf{p}=(\pi,0)$ in the course of the flow toward $\Lambda=0$. It thus turns out that the truncation scheme is insufficient to generate a strong pseudofermion damping and a nonmagnetic phase. This can be traced to the violation of Ward identities in this approximation.

An improved approximation including self-energy effects in the single-scale propagator has been suggested by Katanin.[37] There the single-scale propagator is replaced by the total derivative of the Green's function with respect to Λ. We find that the latter approach, even if only implemented on the one-loop level, reproduces features of the mean-field theory and fulfills the Ward identities exactly, if the RPA-like contributions in the particle-hole channel are considered only.[37,38] In our calculations, we include the additional terms on the right side of the equation for the two-particle vertex in Fig. 8. Calculating the susceptibility, we are now able to distinguish between the three phases. In particular, we get a convergent flow down to $\Lambda=0$ in the region where the paramagnetic phase is expected. The phase boundary between Néel-order and paramagnetic phases is found to be at $g_{c1}\approx 0.4\ldots 0.45$ and the transition from paramagnetism to Collinear order happens at $g_{c2}\approx 0.66\ldots 0.68$. Our findings agree well with the results obtained by other methods.[18,20,21,28,44,46] Approaching the transition to Collinear order, we observe a smooth divergence of the corresponding susceptibility. On the other hand, near the transition to Néel order a different picture emerges. Here it is difficult to access the critical region because the discretization of the frequencies generates large oscillations in the flow at small Λ.

Finally we probed the nonmagnetic phase with respect to columnar dimerization and plaquette order by investigating the flow in the presence of appropriate small perturbative fields. In the limit $\Lambda=0$, the correlations for both types of order are enhanced but a divergence is not found. These results indicate either strong dimer and plaquette fluctuations in a spin-liquid phase or a symmetry-broken phase with dimer or plaquette order.

The work reported here shows that in spite of the fact that quantum spin models are in the strong-coupling regime by definition, partial resummations of perturbation theory appear to capture the physics of frustrated magnets at least on a qualitative level. The resummations, done here in the framework of the functional renormalization-group method, account in a controlled and systematic way for all two-particle interaction processes, including all couplings between the different channels. If self-energy corrections are added in a consistent way, thereby including certain contributions of the three-particle vertex, it appears to be possible to calculate the central quantity of frustrated spin systems in the language of pseudoparticles, the damping of the pseudofermions in a controlled way. The systems we consider are, in principle, infinitely large but the spin correlations are only treated up to some finite length. Hence we do not have to deal with the effects of edges or periodic boundary conditions. However, the range over which our correlations extend typically include more than 200 sites which is much more than the system sizes accessible by exact diagonalization. Furthermore, we do not make any assumption on the ground state or perform an expansion around any presumed state. Our starting point of free fermions without dispersion is completely featureless. Therefore, our approach is straightforwardly applicable to a variety of models. Some obvious extensions of the present work are (1) consideration of other models such as the spin-1/2 J_1-J_2-J_3 Heisenberg antiferromagnet on the square lattice or geometrically frustrated models like the triangular or Kagome lattice, (2) generalization to finite temperature, and (3) calculation of dynamical spin-correlation functions. Work in this direction is in progress.

ACKNOWLEDGMENTS

We thank W. Brenig, R. Thomale, H. Schmidt, M. Salmhofer, and S. Andergassen for stimulating discussions. Financial support by the Deutsche Forschungsgemeinschaft through the Forschergruppe FOR 960 is gratefully acknowledged.

APPENDIX: FRG EQUATIONS WITH FULL DYNAMICS

In this appendix, we show the flow equations for γ, Γ_s, and Γ_d with all frequency dependences,

$$\frac{d}{d\Lambda}\gamma^{\Lambda}(\omega)=\frac{1}{2\pi}\Bigg\{-2\sum_{j}\left[\Gamma^{\Lambda}_{\mathrm{d}\,ij}(\omega+\Lambda,0,\omega-\Lambda)-\Gamma^{\Lambda}_{\mathrm{d}\,ij}(\omega-\Lambda,0,\omega+\Lambda)\right]$$
$$+3\left[\Gamma^{\Lambda}_{\mathrm{s}\,ii}(\omega+\Lambda,\omega-\Lambda,0)-\Gamma^{\Lambda}_{\mathrm{s}\,ii}(\omega-\Lambda,\omega+\Lambda,0)\right]$$
$$+\Gamma^{\Lambda}_{\mathrm{d}\,ii}(\omega+\Lambda,\omega-\Lambda,0)-\Gamma^{\Lambda}_{\mathrm{d}\,ii}(\omega-\Lambda,\omega+\Lambda,0)\Bigg\}\frac{1}{\Lambda+\gamma^{\Lambda}(\Lambda)}, \tag{A1}$$

$$\frac{d}{d\Lambda}\Gamma^{\Lambda}_{\mathrm{s}\,i_1i_2}(s,t,u)=\frac{1}{2\pi}\int_{-\infty}^{\infty}d\omega'\{[-2\Gamma^{\Lambda}_{\mathrm{s}\,i_1i_2}(s,-\omega_{2'}-\omega',\omega_{1'}+\omega')\Gamma^{\Lambda}_{\mathrm{s}\,i_1i_2}(s,\omega_2+\omega',\omega_1+\omega')$$
$$+\Gamma^{\Lambda}_{\mathrm{s}\,i_1i_2}(s,-\omega_{2'}-\omega',\omega_{1'}+\omega')\Gamma^{\Lambda}_{\mathrm{d}\,i_1i_2}(s,\omega_2+\omega',\omega_1+\omega')$$
$$+\Gamma^{\Lambda}_{\mathrm{d}\,i_1i_2}(s,-\omega_{2'}-\omega',\omega_{1'}+\omega')\Gamma^{\Lambda}_{\mathrm{s}\,i_1i_2}(s,\omega_2+\omega',\omega_1+\omega')]$$
$$\times[P^{\Lambda}(\omega',s+\omega')+P^{\Lambda}(s+\omega',\omega')]$$
$$+\Bigg[2\sum_{j}\Gamma^{\Lambda}_{\mathrm{s}\,i_1j}(\omega_{1'}+\omega',t,\omega_1-\omega')\Gamma^{\Lambda}_{\mathrm{s}\,ji_2}(\omega_2+\omega',t,-\omega_{2'}+\omega')$$
$$+\Gamma^{\Lambda}_{\mathrm{s}\,i_1i_2}(\omega_{1'}+\omega',t,\omega_1-\omega')\Gamma^{\Lambda}_{\mathrm{s}\,i_1i_1}(\omega_2+\omega',-\omega_{2'}+\omega',t)$$
$$-\Gamma^{\Lambda}_{\mathrm{s}\,i_1i_2}(\omega_{1'}+\omega',t,\omega_1-\omega')\Gamma^{\Lambda}_{\mathrm{d}\,i_1i_1}(\omega_2+\omega',-\omega_{2'}+\omega',t)$$
$$+\Gamma^{\Lambda}_{\mathrm{s}\,i_1i_1}(\omega_{1'}+\omega',\omega_1-\omega',t)\Gamma^{\Lambda}_{\mathrm{s}\,i_1i_2}(\omega_2+\omega',t,-\omega_{2'}+\omega')$$
$$-\Gamma^{\Lambda}_{\mathrm{d}\,i_1i_1}(\omega_{1'}+\omega',\omega_1-\omega',t)\Gamma^{\Lambda}_{\mathrm{s}\,i_1i_2}(\omega_2+\omega',t,-\omega_{2'}+\omega')\Bigg]$$
$$\times[P^{\Lambda}(\omega',t+\omega')+P^{\Lambda}(t+\omega',\omega')]$$
$$-[2\Gamma^{\Lambda}_{\mathrm{s}\,i_1i_2}(\omega_{2'}-\omega',-\omega_1-\omega',u)\Gamma^{\Lambda}_{\mathrm{s}\,i_1i_2}(\omega_2-\omega',\omega_{1'}+\omega',u)$$
$$+\Gamma^{\Lambda}_{\mathrm{s}\,i_1i_2}(\omega_{2'}-\omega',-\omega_1-\omega',u)\Gamma^{\Lambda}_{\mathrm{d}\,i_1i_2}(\omega_2-\omega',\omega_{1'}+\omega',u)$$
$$+\Gamma^{\Lambda}_{\mathrm{d}\,i_1i_2}(\omega_{2'}-\omega',-\omega_1-\omega',u)\Gamma^{\Lambda}_{\mathrm{s}\,i_1i_2}(\omega_2-\omega',\omega_{1'}+\omega',u)]$$
$$\times[P^{\Lambda}(\omega',u+\omega')+P^{\Lambda}(u+\omega',\omega')]\}, \tag{A2}$$

$$\frac{d}{d\Lambda}\Gamma^{\Lambda}_{\mathrm{d}\,i_1i_2}(s,t,u)=\frac{1}{2\pi}\int_{-\infty}^{\infty}d\omega'\{[3\Gamma^{\Lambda}_{\mathrm{s}\,i_1i_2}(s,-\omega_{2'}-\omega',\omega_{1'}+\omega')\Gamma^{\Lambda}_{\mathrm{s}\,i_1i_2}(s,\omega_2+\omega',\omega_1+\omega')$$
$$+\Gamma^{\Lambda}_{\mathrm{d}\,i_1i_2}(s,-\omega_{2'}-\omega',\omega_{1'}+\omega')\Gamma^{\Lambda}_{\mathrm{d}\,i_1i_2}(s,\omega_2+\omega',\omega_1+\omega')]$$
$$\times[P^{\Lambda}(\omega',s+\omega')+P^{\Lambda}(s+\omega',\omega')]$$
$$+\Bigg[2\sum_{j}\Gamma^{\Lambda}_{\mathrm{d}\,i_1j}(\omega_{1'}+\omega',t,\omega_1-\omega')\Gamma^{\Lambda}_{\mathrm{d}\,ji_2}(\omega_2+\omega',t,-\omega_{2'}+\omega')$$
$$-3\Gamma^{\Lambda}_{\mathrm{d}\,i_1i_2}(\omega_{1'}+\omega',t,\omega_1-\omega')\Gamma^{\Lambda}_{\mathrm{s}\,i_1i_1}(\omega_2+\omega',-\omega_{2'}+\omega',t)$$
$$-\Gamma^{\Lambda}_{\mathrm{d}\,i_1i_2}(\omega_{1'}+\omega',t,\omega_1-\omega')\Gamma^{\Lambda}_{\mathrm{d}\,i_1i_1}(\omega_2+\omega',-\omega_{2'}+\omega',t)$$
$$-3\Gamma^{\Lambda}_{\mathrm{s}\,i_1i_1}(\omega_{1'}+\omega',\omega_1-\omega',t)\Gamma^{\Lambda}_{\mathrm{d}\,i_1i_2}(\omega_2+\omega',t,-\omega_{2'}+\omega')$$
$$-\Gamma^{\Lambda}_{\mathrm{d}\,i_1i_1}(\omega_{1'}+\omega',\omega_1-\omega',t)\Gamma^{\Lambda}_{\mathrm{d}\,i_1i_2}(\omega_2+\omega',t,-\omega_{2'}+\omega')\Bigg]$$
$$\times[P^{\Lambda}(\omega',t+\omega')+P^{\Lambda}(t+\omega',\omega')]$$
$$-[3\Gamma^{\Lambda}_{\mathrm{s}\,i_1i_2}(\omega_{2'}-\omega',-\omega_1-\omega',u)\Gamma^{\Lambda}_{\mathrm{s}\,i_1i_2}(\omega_2-\omega',\omega_{1'}+\omega',u)$$
$$+\Gamma^{\Lambda}_{\mathrm{d}\,i_1i_2}(\omega_{2'}-\omega',-\omega_1-\omega',u)\Gamma^{\Lambda}_{\mathrm{d}\,i_1i_2}(\omega_2-\omega',\omega_{1'}+\omega',u)]$$
$$\times[P^{\Lambda}(\omega',u+\omega')+P^{\Lambda}(u+\omega',\omega')]\}. \tag{A3}$$

Note that the frequency parametrization of Eq. (41) is used for Γ_s and Γ_d. The frequencies $\omega_{1'}$, $\omega_{2'}$, ω_1, and ω_2 on the right side stand for the inverse transformations

$$\omega_{1'} = \frac{1}{2}(s+t+u), \quad \omega_{2'} = \frac{1}{2}(s-t-u),$$

$$\omega_1 = \frac{1}{2}(s-t+u), \quad \omega_2 = \frac{1}{2}(s+t-u). \tag{A4}$$

$P^\Lambda(\omega_1,\omega_2)$ denotes a bubble of S^Λ and G^Λ. For the conventional truncation as discussed in Sec. V B, one gets

$$P^\Lambda(\omega_1,\omega_2) \to P^\Lambda_{\rm con}(\omega_1,\omega_2) = \frac{\delta(|\omega_1|-\Lambda)}{\omega_1+\gamma^\Lambda(\omega_1)}\frac{\Theta(|\omega_2|-\Lambda)}{\omega_2+\gamma^\Lambda(\omega_2)}. \tag{A5}$$

In this scheme, the internal integration $\int d\omega' \ldots$ simplifies to $\Sigma_{\omega'=\pm\Lambda}\ldots$. For the Katanin truncation considered in Sec. V C, we get a more complicated expression,

$$P^\Lambda(\omega_1,\omega_2) \to P^\Lambda_{\rm Kat}(\omega_1,\omega_2) = \frac{\delta(|\omega_1|-\Lambda)}{\omega_1+\gamma^\Lambda(\omega_1)}\frac{\Theta(|\omega_2|-\Lambda)}{\omega_2+\gamma^\Lambda(\omega_2)} + \left(\frac{d}{d\Lambda}\gamma^\Lambda(\omega_1)\right)\frac{\Theta(|\omega_1|-\Lambda)}{(\omega_1+\gamma^\Lambda(\omega_1))^2}\frac{\Theta(|\omega_2|-\Lambda)}{\omega_2+\gamma^\Lambda(\omega_2)}. \tag{A6}$$

In both cases, $P^\Lambda(\omega_1,\omega_2)$ is an odd function separately in ω_1 and ω_2. Finally from the comparison between Eqs. (34) and (35), we get the following initial conditions:

$$\gamma^{\Lambda=\infty}(\omega) = 0,$$

$$\Gamma^{\Lambda=\infty}_{{\rm s}\,i_1 i_2}(s,t,u) = \tfrac{1}{4}J_{i_1 i_2}, \quad \Gamma^{\Lambda=\infty}_{{\rm d}\,i_1 i_2}(s,t,u) = 0. \tag{A.7}$$

[1] P. W. Anderson, Mater. Res. Bull. **8**, 153 (1973).
[2] P. W. Anderson, Science **235**, 1196 (1987).
[3] E. Manousakis, Rev. Mod. Phys. **63**, 1 (1991).
[4] B. B. Beard, R. J. Birgeneau, M. Greven, and U. J. Wiese, Phys. Rev. Lett. **80**, 1742 (1998).
[5] D. P. Arovas and A. Auerbach, Phys. Rev. B **38**, 316 (1988).
[6] S. Chakravarty, B. I. Halperin, and D. R. Nelson, Phys. Rev. B **39**, 2344 (1989).
[7] P. Chandra and B. Doucot, Phys. Rev. B **38**, 9335 (1988).
[8] M. Inui, S. Doniach, and M. Gabay, Phys. Rev. B **38**, 6631 (1988).
[9] T. R. Thurston, R. J. Birgeneau, M. A. Kastner, N. W. Preyer, G. Shirane, Y. Fujii, K. Yamada, Y. Endoh, K. Kakurai, M. Matsuda, Y. Hidaka, and T. Murakami, Phys. Rev. B **40**, 4585 (1989).
[10] G. Khaliullin and P. Horsch, Phys. Rev. B **47**, 463 (1993).
[11] R. Melzi, P. Carretta, A. Lascialfari, M. Mambrini, M. Troyer, P. Millet, and F. Mila, Phys. Rev. Lett. **85**, 1318 (2000).
[12] P. Carretta, R. Melzi, N. Papinutto, and P. Millet, Phys. Rev. Lett. **88**, 047601 (2002).
[13] Q. Si and E. Abrahams, Phys. Rev. Lett. **101**, 076401 (2008).
[14] Q. Si, E. Abrahams, J. Dai, and J. X. Zhu, New J. Phys. **11**, 045001 (2009).
[15] G. M. Zhang, Y. H. Su, Z. Y. Lu, Z. Y. Weng, D. H. Lee, and T. Xiang, EPL **86**, 37006 (2009).
[16] J. Dai, Q. Si, J. X. Zhu, and E. Abrahams, Proc. Natl. Acad. Sci. U.S.A. **106**, 4118 (2009).
[17] A. V. Dotsenko and O. P. Sushkov, Phys. Rev. B **50**, 13821 (1994).
[18] H. J. Schulz, T. A. L. Ziman, and D. Poilblanc, J. Phys. I **6**, 675 (1996).
[19] J. Sirker, Z. Weihong, O. P. Sushkov, and J. Oitmaa, Phys. Rev. B **73**, 184420 (2006).
[20] R. Darradi, O. Derzhko, R. Zinke, J. Schulenburg, S. E. Krüger, and J. Richter, Phys. Rev. B **78**, 214415 (2008).
[21] L. Isaev, G. Ortiz, and J. Dukelsky, Phys. Rev. B **79**, 024409 (2009).
[22] N. Read and S. Sachdev, Phys. Rev. Lett. **66**, 1773 (1991).
[23] L. Capriotti, F. Becca, A. Parola, and S. Sorella, Phys. Rev. B **67**, 212402 (2003).
[24] M. E. Zhitomirsky and K. Ueda, Phys. Rev. B **54**, 9007 (1996).
[25] O. A. Starykh and L. Balents, Phys. Rev. Lett. **93**, 127202 (2004).
[26] P. Sindzingre, Phys. Rev. B **69**, 094418 (2004).
[27] A. A. Nersesyan and A. M. Tsvelik, Phys. Rev. B **67**, 024422 (2003).
[28] O. P. Sushkov, J. Oitmaa, and Z. Weihong, Phys. Rev. B **63**, 104420 (2001).
[29] O. P. Sushkov, J. Oitmaa, and Z. Weihong, Phys. Rev. B **66**, 054401 (2002).
[30] T. Senthil, A. Vishwanath, L. Balents, S. Sachdev, and M. P. A. Fisher, Science **303**, 1490 (2004).
[31] A. A. Abrikosov, Physics (Long Island City, N.Y.) **2**, 5 (1965).
[32] I. Affleck and J. B. Marston, Phys. Rev. B **37**, 3774 (1988).
[33] D. S. Rokhsar and S. A. Kivelson, Phys. Rev. Lett. **61**, 2376 (1988).
[34] P. W. Anderson, P. A. Lee, M. Randeria, T. M. Rice, N. Trivedi, and F. C. Zhang, J. Phys.: Condens. Matter **16**, R755 (2004).
[35] J. Brinckmann and P. A. Lee, Phys. Rev. B **65**, 014502 (2001).
[36] M. Inui, S. Doniach, P. J. Hirschfeld, and A. E. Ruckenstein, Phys. Rev. B **37**, 2320 (1988).
[37] A. A. Katanin, Phys. Rev. B **70**, 115109 (2004).
[38] M. Salmhofer, C. Honerkamp, W. Metzner, and O. Lauscher, Prog. Theor. Phys. **112**, 943 (2004).
[39] J. Brinckmann and P. Wölfle, Phys. Rev. B **70**, 174445 (2004).
[40] J. Brinckmann and P. Wölfle, Physica B **359-361**, 798 (2005).
[41] S. Sachdev, *Quantum Phase Transitions* (Cambridge University Press, Cambridge, England, 1999).
[42] T. Senthil, L. Balents, S. Sachdev, A. Vishwanath, and M. P. A. Fisher, Phys. Rev. B **70**, 144407 (2004).
[43] E. Dagotto and A. Moreo, Phys. Rev. Lett. **63**, 2148 (1989).
[44] T. Einarsson and H. J. Schulz, Phys. Rev. B **51**, 6151 (1995).

[45] R. F. Bishop, D. J. J. Farnell, and J. B. Parkinson, Phys. Rev. B **58**, 6394 (1998).
[46] R. R. P. Singh, Z. Weihong, C. J. Hamer, and J. Oitmaa, Phys. Rev. B **60**, 7278 (1999).
[47] L. Capriotti and S. Sorella, Phys. Rev. Lett. **84**, 3173 (2000).
[48] L. Siurakshina, D. Ihle, and R. Hayn, Phys. Rev. B **64**, 104406 (2001).
[49] L. Capriotti, F. Becca, A. Parola, and S. Sorella, Phys. Rev. Lett. **87**, 097201 (2001).
[50] M. Mambrini, A. Läuchli, D. Poilblanc, and F. Mila, Phys. Rev. B **74**, 144422 (2006).
[51] M. P. Gelfand, Phys. Rev. B **42**, 8206 (1990).
[52] J. W. Negele and H. Orland, *Quantum Many-Particle Systems* (Addison-Wesley, Reading, MA, 1988).
[53] G. Rickayzen, *Green's Functions and Condensed Matter* (Academic Press, New York, 1980).
[54] V. N. Popov and S. A. Fedotov, Sov. Phys. JETP **67**, 535 (1988).
[55] M. N. Kiselev and R. Oppermann, JETP Lett. **71**, 250 (2000).
[56] R. Dillenschneider and J. Richert, Phys. Rev. B **73**, 024409 (2006).
[57] C. Wetterich, Phys. Lett. B **301**, 90 (1993).
[58] C. J. Halboth and W. Metzner, Phys. Rev. B **61**, 7364 (2000).
[59] M. Salmhofer and C. Honerkamp, Prog. Theor. Phys. **105**, 1 (2001).
[60] R. Hedden, V. Meden, T. Pruschke, and K. Schönhammer, J. Phys.: Condens. Matter **16**, 5279 (2004).
[61] C. Honerkamp, M. Salmhofer, N. Furukawa, and T. M. Rice, Phys. Rev. B **63**, 035109 (2001).
[62] C. Karrasch, R. Hedden, R. Peters, T. Pruschke, K. Schönhammer, and V. Meden, J. Phys.: Condens. Matter **20**, 345205 (2008).
[63] S. Andergassen, T. Enss, V. Meden, W. Metzner, U. Schollwöck, and K. Schönhammer, Phys. Rev. B **70**, 075102 (2004).
[64] J. B. Marston and I. Affleck, Phys. Rev. B **39**, 11538 (1989).
[65] G. Baym and L. P. Kadanoff, Phys. Rev. **124**, 287 (1961).
[66] G. Baym, Phys. Rev. **127**, 1391 (1962).
[67] T. R. Morris, Int. J. Mod. Phys. A **9**, 2411 (1994).
[68] T. Enss, V. Meden, S. Andergassen, X. Barnabé-Thériault, W. Metzner, and K. Schönhammer, Phys. Rev. B **71**, 155401 (2005).
[69] R. Gersch, C. Honerkamp, and W. Metzner, New J. Phys. **10**, 045003 (2008).
[70] R. Gersch, C. Honerkamp, D. Rohe, and W. Metzner, Eur. Phys. J. B **48**, 349 (2005).